NASA TECHNICAL MEMORANDUM

NASA TM X-2734

NASA TM X-2734



# ANALYTICAL STUDY ON A TWO-DIMENSIONAL PLANE OF THE OFF-DESIGN FLOW PROPERTIES OF TANDEM-BLADED COMPRESSOR STATORS

*by Nelson L. Sanger*

*Lewis Research Center*
*Cleveland, Ohio 44135*

NATIONAL AERONAUTICS AND SPACE ADMINISTRATION • WASHINGTON, D. C. • MARCH 1973

| 1. Report No. | 2. Government Accession No. | 3. Recipient's Catalog No. |
|---|---|---|
| NASA TM X-2734 | | |

| 4. Title and Subtitle | 5. Report Date |
|---|---|
| ANALYTICAL STUDY ON A TWO-DIMENSIONAL PLANE OF THE OFF-DESIGN FLOW PROPERTIES OF TANDEM-BLADED COMPRESSOR STATORS | March 1973 |
| | 6. Performing Organization Code |
| 7. Author(s) | 8. Performing Organization Report No. |
| Nelson L. Sanger | E-7031 |
| | 10. Work Unit No. |
| 9. Performing Organization Name and Address | 501-24 |
| Lewis Research Center<br>National Aeronautics and Space Administration<br>Cleveland, Ohio 44135 | 11. Contract or Grant No. |
| | 13. Type of Report and Period Covered |
| 12. Sponsoring Agency Name and Address | Technical Memorandum |
| National Aeronautics and Space Administration<br>Washington, D.C. 20546 | 14. Sponsoring Agency Code |

15. Supplementary Notes

16. Abstract

The flow characteristics of several tandem-bladed compressor stators were analytically evaluated over a range of inlet incidence angles. The ratios of rear-segment to front-segment chord and camber were varied. Results were also compared to the analytical performance of a reference solid blade section. All tandem blade sections exhibited lower calculated losses than the solid stator. But no one geometric configuration exhibited clearly superior characteristics. The front segment accepts the major effect of overall incidence-angle change. Rear- to front-segment camber ratios of 4 and greater appeared to be limited by boundary-layer separation from the pressure surface of the rear segment.

17. Key Words (Suggested by Author(s))

Compressors
Turbomachinery
Turbomachine blades
Stator blades
Airfoil aerodynamics

18. Distribution Statement

Unclassified - unlimited

| 19. Security Classif. (of this report) | 20. Security Classif. (of this page) | 21. No. of Pages | 22. Price* |
|---|---|---|---|
| Unclassified | Unclassified | 41 | $3.00 |

* For sale by the National Technical Information Service, Springfield, Virginia 22151

# ANALYTICAL STUDY ON A TWO-DIMENSIONAL PLANE OF THE OFF-DESIGN FLOW PROPERTIES OF TANDEM-BLADED COMPRESSOR STATORS

by Nelson L. Sanger

Lewis Research Center

## SUMMARY

The flow characteristics of several tandem-bladed compressor stators were analytically evaluated over a range of inlet incidence angles. The ratios of rear-segment to front-segment chord and camber were systematically varied. Results were also compared to the analytical performance of a reference solid blade section.

The solid and tandem blade sections were designed to have the same overall camber, total chord length, solidity, and inlet velocity triangles. The solid blade design diffusion factor D was 0.5.

The study utilized several analytical procedures. Blade-surface and flow-field velocities were computed by an ideal-flow method for several values of inlet flow angle. Boundary-layer growth on each blade surface and forces on each segment were computed separately; both calculation procedures used analytical surface velocities as input. A total-pressure-loss coefficient was computed by using calculated values of boundary-layer displacement and momentum thickness. The study was conducted on a two-dimensional flow plane and used double-circular-arc stator blade sections.

All tandem-bladed sections investigated exhibited lower calculated losses than the reference solid stator section over the range of incidence angle investigated. Based on loss, no one geometric configuration exhibited clearly superior characteristics.

Changes in overall incidence angle resulted in significant increases in blade surface-velocity gradients and loss across the front segment but in negligible change in either parameter across the rear segment. It is therefore desirable to favor designs having relatively high rear-segment loadings (i.e., low front-segment loadings) for off-design operation.

As front-segment chord length was reduced, the flow around the rear-segment leading edge showed increasingly direct effects of change in overall incidence angle. This is a direct reflection of the guidance effect provided by the front-segment pressure surface and an indication that very short front segments should be avoided for off-design applications.

The ratio of rear- to front-segment camber angle showed evidence of being limited above values of 4 by strong rear segment pressure surface velocity diffusions which produced boundary layer separation.

# INTRODUCTION

Aircraft engines of the future will require more-compact, lighter weight compressors capable of maintaining high performance levels over a wide range of operating conditions. More work per blade (higher loading) will be required without a sacrifice in efficiency and stable operating range. The tandem blade concept is one possible means of achieving this objective. Experimental evidence indicates that some tandem blade designs are capable of sustaining high loading with relatively small losses (refs. 1 to 4).

The effects on performance of important tandem blade geometric parameters were analytically studied in reference 5. A highly loaded compressor stator application (diffusion factor, D = 0.5) was analyzed at design-point conditions. It was shown that tandem-bladed stators can have lower calculated losses than an equivalent conventional solid blade if certain geometric parameters are controlled.

However, it is equally important for a blade row to operate over a range of inlet flow conditions. Maneuvering operations, inlet flow distortions, and flight at different altitudes and speeds all require the fan and compressor to accept a variety of off-design flow conditions. Therefore, in the present report, the tandem blade study is carried a step further. This investigation has as its objective to determine (1) if a tandem blade section designed according to the recommendations of reference 5 can show an analytical performance advantage over conventional solid blade sections at off-design flow conditions and (2) if there are specific tandem blade configurations which are markedly superior to others for off-design operation.

A solid blade section used as a reference blade in this study is the same as used in reference 5. Seven tandem blade sections were designed using the general geometric recommendations of reference 5. All blade sections had the same design inlet velocity triangles and overall camber as the solid blade section. Chord length and camber angle of the tandem front and rear blade segments were systematically varied.

Analytical techniques developed at the Lewis Research Center and programmed for computer use were used to evaluate each design. Blade geometry was obtained from a double-circular-arc blade coordinate program (ref. 6). Blade-surface and flow-field velocities were computed by an ideal-flow program (ref. 7). Boundary-layer development on each blade surface and forces on each segment were computed by separate programs (refs. 8 and 9). And total-pressure-loss coefficient was computed by using Stewart's method (ref. 10). Incidence angle was varied over the same range for each of the tandem configurations having different ratios of segment chord and for each of the configurations having different camber ratios. The effects of changes in flow and geometrical parameters were evaluated by using calculated surface velocities, boundary-layer parameters, total-pressure-loss coefficients, and calculated streamline diagrams. The study was conducted on a two-dimensional blade-to-blade flow plane using double-circular-arc stator blade sections.

# DESIGN

The design parameters for the solid stator blade sections used as reference in this study were

(1) Diffusion factor, D, 0.5

(2) Overall camber, $\varphi$, $58.8^{\circ}$

(3) Fluid turning, $\Delta\beta$, $43.25^{\circ}$

(4) Solidity, $\sigma$, 1.5

(5) Total chord, $C_T$, 0.102 m

Double-circular-arc blade shapes were used throughout, and all blade sections lay on two-dimensional planes. The inlet axial velocity at the design incidence angle was 76.3 meters per second, and the entire flow field was subsonic. The blade design procedure is described in reference 5. Tandem blade sections had identical inlet velocity triangle, overall solidity, overall camber, and total chord as the solid blade section. The overall blade-section geometry parameters used in the design of both the solid and tandem blades are defined in figure 1. The design parameters for the solid and tandem blade sections are given in table I. All symbols are defined in the appendix.

The tandem blade sections are composed of two blade segments called the front segment and the rear segment. Both segments are composed of double-circular-arc shapes. Values for maximum thickness, leading-edge radius, and trailing-edge radius expressed as percentage of local chord (i.e., of front- or rear-segment chords) were identical to analogous solid blade section parameters expressed as percentage of total chord. Blade coordinates for solid and tandem blades were obtained from the program of reference 6.

Geometrical parameters of the tandem blade section are shown in figure 2. They are

(1) Channel convergence, F - the ratio of inlet (capture area) to outlet area of the channel between segments

(2) Overlap, L - the length of channel from the rear-segment leading-edge center of radius to the front-segment trailing-edge center of radius

(3) Gap, G - the width of the channel at its exit

(4) Camber ratio, $\varphi_R/\varphi_F$ - the ratio of the rear-segment camber angle to the front-segment camber angle

(5) Chord ratio, $C_R/C_F$ - the ratio of the rear-segment chord to the front-segment chord

(6) Rear-segment relative setting angle, $\kappa_{b-b}$ - the difference between the direction of the meanline of the rear segment at the leading edge and the direction of the meanline of the front segment at the point of intersection with the line $F \times G$ (see fig. 2)

Gap and overlap are referenced to the total chord to make all parameters dimensionless.

The effect of variation of each of these geometric parameters on blade performance was investigated in reference 5. Results showed that surface velocity diffusion and flow losses could be reduced when convergence F was relatively small ($1.0 < F < 1.2$), gap G was relatively small ($0.027 < G/C_T < 0.056$), overlap L was relatively large ($0.112 < L/C_T < 0.251$), camber ratio $\varphi_R/\varphi_F \sim 2$, chord ratio $C_R/C_F \sim 1$, and rear-segment relative setting angle $\kappa_{b\text{-}b} \sim -5^\circ$. These results were used in the design of the tandem blade sections for the present study. The variation of tandem blade geometrical parameters is as follows:

| | |
|---|---|
| Channel convergence, F | 1.1, 1.2 |
| Overlap-chord ratio, $L/C_T$ | 0.11 |
| Gap-chord ratio, $G/C_T$ | 0.04 |
| Camber ratio, $\varphi_R/\varphi_F$ | 1, 2, 3 |
| Chord ratio, $C_R/C_F$ | 1, 1.5, 2, 3 |

The resulting geometrical configurations are described in table II.

All parameters remained within the guidelines of reference 5 except chord ratio and camber ratio, which were varied systematically. Two values of convergence F were used, 1.1 and 1.2 (see table II). It was necessary to increase convergence to 1.2 for the camber ratio configurations in order to keep $\kappa_{b\text{-}b}$ at levels close to $-5^\circ$ ($\kappa_{b\text{-}b}$ is not an independent variable but is dependent on convergence and segment camber angles).

## ANALYTICAL PROCEDURE

Four analytical procedures were used in the study. Velocity distributions (blade surface and blade-to-blade flow field) were obtained from an inviscid flow calculation. The surface velocities were used to compute boundary-layer growth, from which loss calculations were made. Pressure forces were calculated on all blade segments at design flow conditions.

### Ideal-Flow Calculations

Two ideal-flow programs were used: one for the solid blade (ref. 11) and the other for the tandem blades (ref. 7). The programs solve the stream function equation by finite difference methods. The flow field is compressible, subsonic, two dimensional, and nonviscous. A constant blade-to-blade stream channel height in the radial direction

was used. The input includes blade geometry, fluid properties, flow rate, inlet and outlet flow angles, and the finite difference grid. The output includes surface velocities and blade-to-blade flow field velocities and fluid angles.

Inlet angle was varied in the positive direction from the design value (referred to subsequently as the reference value). A further explanation of this procedure is given in the section Analytical Limitations. Inlet velocity to the blade was maintained constant as inlet angle was changed. The inlet conditions were total pressure, 10.1 $N/cm^2$; total temperature, 518.7° R; total density, 0.000981 $kg/m^3$; and inlet velocity, 104.5 m/sec.

Because the solution to the stream function equation is of the boundary-value type, the percentage of weight flow through the channel between tandem segments must be specified in the tandem blade program, and the outlet flow angle must be specified in both the solid blade and tandem blade programs. Generally, these are both unknown variables. In this study, outlet angle and tandem channel weight flow were determined by an iterative procedure. The criterion to be met was that the suction-surface and pressure-surface velocities must be equal at the trailing edge (surface-velocity diagram closed). This assumes that a blade or blade segment is completely loaded to the trailing edge (i.e., no crossing of surface velocities before the trailing edge) and that no pressure gradient will be supported beyond the trailing edge (i.e., surface-velocity diagram cannot be open at the trailing edge).

## Boundary-Layer Calculations

The blade surface velocities computed by the ideal-flow programs were used to calculate the boundary-layer growth by using the program of reference 8. An integral boundary-layer calculation method is used to solve the two-dimensional compressible laminar- or turbulent-boundary-layer equations in an arbitrary pressure gradient. Many options are available to the user which require the user to make certain assumptions. The assumptions made for this investigation relate to whether the boundary layer is initially laminar or turbulent, to the initial thickness values used, and to the selection of a turbulent separation criterion.

The boundary layer was assumed turbulent over the entire blade surface. In real compressors, high turbulence levels, surface roughness effects, and leading-edge effects act to force either early transition or laminar separation followed by turbulent reattachment.

The boundary-layer program calculates the turbulent boundary layer by using Sasman and Cresci's integral method (ref. 12). This method requires initial values for displacement and momentum thickness. Because of the size of actual compressor blades, accurate boundary-layer measurements near the leading edge are difficult to

obtain. For use in this investigation, measurements made by Becker (ref. 13) on a wing having a 1.5-meter chord were scaled down. The resulting initial displacement thickness was 0.00609 centimeter and the momentum thickness was 0.00436 centimeter. These values were applied consistently to all blade configurations considered.

The parameter used to predict turbulent separation was the incompressible form factor $H_i$. Boundary-layer and compressor literature cite critical values of $H_i$, ranging from 1.8 to 2.6. A value of 2.0 is used most often to indicate turbulent separation and was so used in this study.

## Loss Calculations

Stewart's method (ref. 10) was used to calculate the total compressible flow loss caused by blade friction, trailing-edge thickness, and downstream mixing. The total loss coefficient $\overline{\omega}_T$ is defined as the total pressure loss across the blade row divided by the inlet dynamic head. The analytical expression for $\overline{\omega}_T$ depends on displacement and momentum thickness at the blade trailing edge, blade trailing-edge thickness, fluid exit angle, exit velocity, and fluid properties. For analytical computations the exit velocity, exit angle, and fluid properties are available from the ideal-flow calculations; trailing-edge thickness is known; and displacement and momentum thickness are available from the boundary-layer calculations. When separation was indicated, the boundary-layer thicknesses were extrapolated to the trailing-edge station.

## Force Calculations

The surface-velocity distributions calculated in the ideal-flow programs were used to compute the pressure forces on each blade segment (ref. 9) at the design point only. The surface velocities converted to pressure are integrated by the trapezoidal rule over each surface, and the resultant forces are resolved into the tangential and meridional directions. The ratio between rear-segment and front-segment tangential force components $\left(f_R/f_F\right)_\theta$ can be thought of as a work split (for rotating blade rows) or a circulation split (for stationary blade rows). For the sake of simplicity, it is referred to herein as a work split, even though a stationary blade row is under consideration.

## Analytical Limitations

Restriction to positive incidence angles. - Comparisons between solid and tandem

blades were restricted to operation at positive incidence angles. As incidence angle becomes increasingly negative, tandem blade boundary-layer behavior becomes increasingly difficult to interpret. Some of the factors influencing this interpretation are discussed in this section.

On the suction surface of either segment of a tandem blade or on a solid blade suction surface, flow accelerates and then decelerates, causing the boundary layer to grow continually until it reaches the trailing edge or separates. On the front-segment pressure surface of a tandem blade the flow decelerates and then accelerates through the channel between the two segments. The boundary layer grows and then diminishes as it passes through the channel region. At some critical negative incidence angle the deceleration will cause the boundary layer to separate, thus preventing flow through the channel between blade segments. The greatly altered flow pattern will most likely result in large losses.

To accurately determine the critical negative incidence angle analytically is difficult because it is sensitive to the assumptions for initial displacement thickness and for incompressible form factor at separation. In effect, these assumptions determine whether separation will be predicted, instead of at what location on the blade surface it will be predicted, as is the case for suction-surface boundary layers. A qualitative example of these effects is shown in figure 3, where incompressible form factor is plotted for three values of initial boundary-layer thickness. The smallest value, 0.00609 centimeter, was used in all cases investigated in the present study. The other values represent two times and three times this initial value. The same surface-velocity distribution was used for all cases. If the separation criterion of $H_i = 2.0$ used in the present study was applied, separation would be predicted for the largest initial thickness, would not be predicted for the smallest, and would be a borderline case for the thickness midway between. Therefore, the choice of initial thickness would be important in determining whether separation would be predicted.

It is also apparent from figure 3 that, for any given initial thickness, the value of incompressible form factor selected as the separation criterion would be critical. An $H_i$ of 2.2 or 2.4, for example, would predict separation only for the largest initial thickness shown.

The flow over the pressure surface of a solid blade at negative incidence produces a similar effect, but with less severe consequences. The adverse pressure gradient near the leading edge at negative incidence is steep and tends to produce rapid growth of boundary-layer thickness and form factor. Downstream from the leading edge the pressure gradient is reduced and a separated boundary layer may reattach. But even if reattachment does not occur, the major alteration in the flow field associated with tandem blades is not likely to be found in solid blades.

The same kind of uncertainty is not present for positive values of $i - i_{ref}$. A simi-

lar flow situation does not exist. If initial $\delta^*$ or critical $H_i$ are changed, the effect will be to raise or lower the overall level of loss, but not to create an abrupt excursion. Therefore, only positive-incidence-angle calculations are presented.

Absolute values of loss coefficient. - Whenever possible, total-pressure-loss coefficient is expressed in a ratio form. The purpose of this is to emphasize that tandem blade configurations are to be compared among themselves and to a reference solid blade. It is recognized that the ability to predict loss coefficient quantitatively is hampered both by the quasi-arbitrary choice of initial-boundary-layer thickness and by the lack of a loss model which incorporates the effect of a separated boundary layer (necessitating an extrapolation of boundary-layer thicknesses to the trailing-edge station to obtain input to the loss calculation).

The loss parameter used herein provides a convenient single-parameter basis for comparison. The alternative to using this imperfect loss model is to attempt to identify trends by comparing boundary-layer growth and thickness values on each configuration for several incidence angles. The complexity of such a task is made evident by considering that the solid blade has two boundary layers and each tandem configuration has four. Therefore, the loss coefficient was chosen as the single parameter which incorporates the combined effects of the boundary layers; and then the same boundary-layer assumptions and methods were employed on each configuration.

## RESULTS AND DISCUSSION

The analytical performance of the solid stator and seven tandem-bladed stators is evaluated at several off-design flow conditions in this section. The solid blade analysis is presented first to establish a reference condition. The effect of change in chord ratio on tandem blade off-design performance is considered next, and finally, the effect of change in camber ratio is evaluated.

For each configuration studied, a standard format of plots is presented. Most parameters are presented in nondimensional form. The types of plots are

(1) Velocity distributions on blade suction and pressure surfaces, presented nondimensionally as $W_S/W_{z,1}$ where $W_S$ is the blade surface velocity and $W_{z,1}$ is the axial component of the inlet velocity

(2) Boundary-layer growth on the blade surfaces as measured by displacement thickness and incompressible form factor

(3) Loss coefficient $\overline{\omega}$ on front and rear tandem blade segments, and a total loss which is a summation of the individual segment losses, expressed as $\overline{\omega}/\overline{\omega}_{s,0}$ where $\overline{\omega}_{s,0}$ is the solid blade loss coefficient at $i - i_{ref} = 0$ (design point)

(4) The work split between tandem rear and front blade segments at design inlet

angle, as measured by the ratio of tangential forces $\left(f_R/f_F\right)_\theta$

The data on the plots are generally self-explanatory and the plots are not discussed individually. Instead, they are used as necessary to illustrate certain general or specific trends. Surface-velocity and boundary-layer plots are computer-generated microfilm plots. Successive points are connected by straight lines and may account for the lack of smoothness in some areas.

## Solid Blade

Surface velocities at different inlet incidence angles are plotted in figure 4. It should be noted that since the inlet velocity is held constant for all conditions, the axial inlet velocity $W_{z,1}$ does change as inlet angle changes. The anticipated increase in velocity diffusion on the suction surface with increase in incidence angle is evident from the curves.

The boundary-layer parameters, incompressible form factor and displacement thickness, are presented in figure 5. The trend of earlier separation on the suction surface as incidence angle is increased is shown by the intersection of the line $H_i = 2.0$ with the respective curves. It is evident from a comparison of figures 4 and 5 that the criterion used to specify potential flow exit angle has a direct influence on boundary-layer behavior (through the surface velocities) in the trailing-edge regions. And this effect is necessarily carried through to the loss calculation. The trend of loss with incidence angle, presented in figure 6, indicates that loss would double from design value at about $10^\circ$ of positive incidence.

## Tandem Blades

All the tandem configurations were evaluated over the same range of incidence angle. Two geometric parameters were varied to determine their effect on off-design performance. The variation of chord ratio and the variation of camber ratio are discussed in that order.

Variation of chord ratio. - Tandem blade configurations having chord ratios $C_R/C_F$ of 1, 1.5, 2, and 3 were evaluated. Section geometry of each is shown in figure 7 and tabulated in table II.

The surface-velocity and boundary-layer plots, shown in figures 8 to 15, illustrate clearly that the front segment of a tandem blade accepts the major effect of change in incidence angle. A further effect shown is that as chord ratio is increased (front-segment chord becomes shorter) the diffusion over the front-segment suction surface

increases (compare slopes of $W_S/W_{z,1}$ against distance at equal $i - i_{ref}$ values). Although this leads to earlier boundary-layer separation for high-chord-ratio configurations, the boundary-layer thickness at separation is considerably smaller than for low-chord-ratio configurations, because of the shorter chord length (shorter surface length for boundary-layer development). There are, therefore, two offsetting effects. Nevertheless, separation from the front segment is a condition to be avoided, or at least, delayed. The separated wake will mix with fluid downstream and thereby may adversely affect boundary-layer flow over the rear-segment suction surface. Since separation is more likely to occur when front-segment chords are short, the relatively long distance over the length of the rear segment presents ample opportunity for the wake to mix with the surface boundary layer.

It can also be observed from figure 8 that rear-segment diffusion is not noticeably affected by change in incidence angle for low-chord-ratio configurations. However, for high-chord-ratio configurations the rear-segment diffusion increases with increasing overall incidence (fig. 14). This effect is also reflected in the boundary-layer calculations by an increase in $\delta^*$ and in an earlier separation point on the rear segment. The reverse trend is seen to occur on the rear-segment pressure surface; that is, diffusion is relieved as overall incidence increases.

Why these effects occur can perhaps best be seen by referring to figure 16. The figure shows the front- and rear-segment inlet stagnation streamlines plotted for two overall incidence angles (corresponding to $i - i_{ref}$ of $0^\circ$ and $+12^\circ$). Two configurations are considered: $C_R/C_F = 1$ and $C_R/C_F = 3$. What is apparent is the guidance effect the front segment provides at off-design conditions. A relatively long front segment ($C_R/C_F = 1$) accepts the full effects of inlet incidence and prevents the rear segment from being affected. When the front segment is short ($C_R/C_F = 3$), the overall inlet angle is transmitted to the rear segment and accounts for the previously observed effects on the rear-segment surface velocities and boundary-layer behavior.

The analytically computed total-pressure-loss coefficient is shown in figure 17 for the front segment, the rear segment, and the combined total loss. In the following discussion it is important to distinguish between the level of loss and the rate of change of loss as incidence angle changes. The front-segment loss levels show a consistent trend with chord ratio. Apparently because of the shorter chord lengths, and despite steeper velocity gradients, the higher-chord-ratio configurations show lower front-segment loss levels over the complete range of incidence angle. But, as incidence angle increases, the rate of change of loss does not differ from one configuration to another. That is, the range properties of the tandem blades (as reflected in front-segment loss) are not affected by chord ratio.

The rear-segment losses do not even show a consistent trend of loss level with chord ratio, although it should be noted that the two configurations having the shortest

front chords ($C_R/C_F$ of 2 and 3), and thus the least guidance effect, do show higher loss levels. These two configurations also have relatively long rear segments, which provide more surface length for boundary-layer growth. Also the $\kappa_{b-b}$ values for both configurations are slightly more positive than desirable, therefore, providing a slightly higher effective incidence angle to the rear segment.

Combining the front- and rear-segment losses yields the total loss. The slopes of the loss against $i - i_{ref}$ curves are essentially the same; and, therefore, no tandem configuration can be clearly identified as having better range properties than another. Also plotted in figure 17 for comparison is the solid-blade-loss curve. One definite conclusion that can be drawn is that all the tandem blade configurations exhibit lower calculated losses than the reference solid blade and a lesser rate of change with incidence over the range of incidence angles investigated.

A measure of work split between tandem blade segments at design incidence angle is presented in figure 18. The ratio of rear-segment to front-segment tangential force is plotted against chord ratio. The shift of loading to the rear segment with increase in chord ratio is caused mainly by an increase in rear-segment chord length, because segment camber angles are essentially constant for all chord ratio configurations (table II).

Variation of camber ratio. - The other principal means of changing the work split between front and rear segments is to change the camber angles of the respective segments, that is, the camber ratio $\varphi_R/\varphi_F$. When total camber angle is fixed, increasing $\varphi_R/\varphi_F$ causes rear camber (and therefore turning) to increase at the expense of front camber (turning). Evidence of this effect is reflected in changes in area under surface-velocity curves and in changes in surface-velocity diffusion. Three tandem configurations having camber ratios $\varphi_R/\varphi_F$ of 2, 3, and 4 were evaluated. Chord ratio was maintained constant at 2. Section geometry of each configuration is shown in figure 19. Surface-velocity and boundary-layer plots are presented in figures 20 to 25.

Examination of the surface-velocity plots reveals two trends. The first is that diffusion over the front-segment suction surface at equal values of $i - i_{ref}$ is less at high camber ratios. This occurs because at high camber ratios, the front camber angle $\varphi_F$ is relatively small. The second trend is the appearance of noticeable diffusion on the rear-segment pressure surface as camber ratio is increased. This is caused mainly by the increased rear camber angle $\varphi_R$, which results in greater streamline distortion in the vicinity of the leading edge. It is noteworthy that this effect is relieved by increasing the overall incidence angle. In general, as was noted for the chord ratio configurations, changes in overall incidence angle had the most significant effects on the front segment, while less significant effects occurred on the rear segment. This general condition points up the desirability of designs having relatively high rear-segment loadings (i.e., low front-segment loadings).

The surface-velocity trends are reflected directly in the boundary-layer behavior.

As camber ratio is increased, the front-segment suction-surface boundary layer separates later ($\varphi_F$ decreases), and the rear-segment suction-surface boundary layer separates earlier ($\varphi_R$ increases). As discussed earlier, delay of separation from the front segment is a condition to strive for. This condition is best met by configurations having relatively high camber ratios. But these configurations are not without problems. The most serious effect shown by the camber ratio configurations occurs on the rear-segment pressure surface (fig. 25(b)). For the $\varphi_R/\varphi_F = 4$ configuration the rear-segment pressure-surface boundary layer would most likely separate for flow conditions associated with $i - i_{ref}$ of $0^o$, $+3^o$, and possibly $+6^o$. Thus, this is not a good configuration for either design flow conditions or off-design conditions where $i - i_{ref}$ is negative (choke conditions) or slightly positive. This illustrates a potential limitation for configurations having highly loaded rear segments, as this one does.

The slopes of the loss curves, shown in figure 26, do not indicate that loss changed with overall incidence angle in any significantly different manner as camber ratio was varied. The levels of loss are different, but they maintain the same relation to each other as overall incidence angle is changed. The trend of segment level of loss follows the trend of individual segment camber (increasing camber, increasing loss). The comparison of total loss with the calculated loss for the reference solid blade also shows all tandem configurations to have lower levels of loss and a lower rate of change of loss with incidence-angle increase.

The only exception to this trend is the configuration $\varphi_R/\varphi_F = 4$, for which (based on the $H_i = 2.0$ criterion) boundary-layer separation on the rear-segment pressure surface would occur for $i - i_{ref}$ of $0^o$, $+3^o$, and possibly $+6^o$. Such separation was not taken into account when the loss calculations were made, so the values for $\varphi_R/\varphi_F = 4$ are probably optimistic. In estimating a correction, one would expect that at small values of $i - i_{ref}$ the pressure-surface separation would add to the loss. Since, as overall incidence is increased, the rear-segment pressure-surface boundary layer becomes less likely to separate, loss corrections would decrease. The resulting loss curve, although higher in level than for other tandem configurations, would exhibit a more level tendency with increasing incidence than is indicated in figure 26.

The work split between rear and front segments at design incidence angle is shown in figure 27. The shift of work (circulation) to the rear segment with an increase in camber ratio is caused mainly by an increase in rear-segment camber angle with a concurrent decrease in front-segment camber angle. Individual segment chord lengths remained essentially constant (table II).

## SUMMARY OF RESULTS

The flow characteristics of several tandem-bladed compressor stators were eval-

uated over a range of inlet incidence angles. The ratios of rear-segment to front-segment chord ratio and camber ratio were systematically varied. Results were also compared to the analytical performance of an equivalent conventional solid blade section.

The reference solid blade section and each tandem blade section were designed to have the same overall camber ($58.8^{\circ}$), total chord length (0.102 m), solidity (1.5), and inlet velocity triangles. The solid blade section was designed for a diffusion factor D of 0.5.

The analysis of each tandem blade configuration included calculation at each incidence angle of ideal flow, boundary-layer growth, and blade segment loss. Forces on each blade segment were calculated at the zero incidence condition to obtain the work split between segments. Specific results of the study include the following:

1. All tandem-bladed stator sections investigated exhibited lower calculated losses than the equivalent solid stator section over the range of incidence angles investigated.

2. Changes in incidence angle result in significant increases in blade surface-velocity gradients and loss across the front segment but in negligible change in either parameter across the rear segment. It is therefore advisable, insofar as it is compatible with other design constraints, to favor designs having relatively high rear- to front-segment work split.

3. The front-segment pressure surface effectively guides the flow approaching the leading edge of the rear segment. For a front segment having a relatively long chord, the velocity diffusion on the rear segment remains the same over a wide range of incidence angle. As the front-segment chord is reduced, the velocity diffusion on the rear segment varies increasingly with incidence changes.

4. Camber ratio showed evidence of being limited above values of 4 by boundary-layer separation from the rear-segment pressure surface. The separated conditions occur at low-to-moderate incidence angles and would impose probable operating penalties at design and choke conditions.

Strictly speaking, the trends and numerical values noted in this study apply only to the configurations evaluated. However, the physical basis underlying the overall trends and trade-offs has general applicability. The study should therefore, at the least, provide the designer with some sound qualitative tools for evaluating widely varying designs.

Lewis Research Center,
National Aeronautics and Space Administration,
Cleveland, Ohio, November 10, 1972,
501-24.

# APPENDIX - SYMBOLS

| | |
|---|---|
| C | blade chord length, m |
| D | diffusion factor |
| F | channel convergence, ratio of gap at inlet to gap at outlet of channel (fig. 2) |
| f | force on blade surface, N |
| G | gap between blade segments (fig. 2), m |
| $H_i$ | incompressible form factor (ref. 8) |
| i | incidence angle (i.e., angle between entrance flow direction and line tangent to blade-section (segment) meanline at leading edge), deg |
| $i_{ref}$ | reference incidence angle; design incidence angle |
| L | overlap between blade segments (fig. 2), m |
| l.e. | leading edge |
| $R_i$ | leading-edge radius of blade segment, m |
| $R_o$ | trailing-edge radius of blade segment, m |
| t | thickness of blade, m |
| te | trailing edge |
| W | velocity, m/sec |
| z | axial coordinate, m |
| $\beta$ | fluid angle with respect to axial direction, deg |
| $\Delta\beta$ | fluid turning angle, deg |
| $\delta^*$ | displacement thickness of boundary layer, m |
| $\theta$ | momentum thickness of boundary layer, m |
| $\kappa$ | blade angle with respect to axial direction, deg |
| $\kappa_{b-b}$ | angle between tangents to mean camber lines of rear blade segment and front blade segment at points of intersection with line containing F × G (fig. 2), deg |
| $\sigma$ | blade solidity (i.e., chord-spacing ratio) |
| $\varphi$ | blade camber, deg |
| $\overline{\omega}$ | blade loss coefficient (i.e., ratio of total pressure loss to inlet dynamic pressure) |

Subscripts:

| | |
|---|---|
| F | front blade segment |
| max | maximum |
| out | conditions at blade trailing edge |
| R | rear blade segment |
| S | surface |
| s, 0 | solid blade at $i - i_{ref} = 0$ |
| T | total or overall conditions |
| t, z | axial projection of total chord |
| z, 1 | axial direction at inlet |
| $\theta$ | tangential direction |
| 1 | blade inlet condition |

# REFERENCES


1. Bettner, James L.; and Nosek, Stanley M.: Summary of Tests on Two Highly Loaded Turbine Blade Concepts in Three-Dimensional Cascade Sector. Paper 69-WA/GT-5, ASME, Nov. 1969.

2. Linnemann, H.: Tandem Grid in a Single Stage Blower. Rep. RSIC-276, Redstone Scientific Information Center, Army Missile Command, Sept. 1964. (Available from DDC as AD-606782.)

3. Railly, J. W.; and El-Sarha, M. E.: An Investigation of the Flow Through Tandem Cascades. Proc. Inst. Mech. Eng., vol. 180, pt. 3J, 1965-66, pp. 66-73.

4. Lueders, H. G.; and Roelke, R. J.: Some Experimental Results of Two Concepts Designed to Increase Turbine Blade Loading. Paper 69-WA/GT-1, ASME, Nov. 1969.

5. Sanger, Nelson L.: Analytical Study of the Effects of Geometric Changes on the Flow Characteristics of Tandem-Bladed Compressor Stators. NASA TN D-6264, 1971.

6. McNally, William D.; and Crouse, James E.: FORTRAN Program for Computing Coordinates of Circular Arc Single and Tandem Turbomachinery Blade Sections on a Plane. NASA TN D-6020, 1970.

7. Katsanis, Theodore; and McNally, William D.: FORTRAN Program for Calculating Velocities on a Blade-to-Blade Stream Surface of a Tandem Blade Turbomachine. NASA TN D-5044, 1969.

8. McNally, William D.: FORTRAN Program for Calculating Compressible Laminar and Turbulent Boundary Layers in Arbitrary Pressure Gradients. NASA TN D-5681, 1970.

9. McNally, William D.: FORTRAN Program for Calculating Aerodynamic Forces from Pressure or Velocity Distributions on Blade Sections. NASA TM X-2123, 1970.

10. Stewart, Warner L.: Analysis of Two-Dimensional Compressible-Flow Loss Characteristics Downstream of Turbomachine Blade Rows in Terms of Basic Boundary-Layer Characteristics. NACA TN 3515, 1955.

11. Katsanis, Theodore; and McNally, William D.: Revised FORTRAN Program for Calculating Velocities and Streamlines on a Blade-to-Blade Stream Surface of a Turbomachine. NASA TM X-1764, 1969.

12. Sasman, Philip K.; and Cresci, Robert J.: Compressible Turbulent Boundary Layer with Pressure Gradient and Heat Transfer. AIAA J. vol. 4, no. 1, Jan. 1966, pp. 19-25.

13. Becker, John V.: Boundary-Layer Transition on the NACA 0012 and 23012 Airfoils in the 8-Foot High-Speed Wind Tunnel. NACA WR-L-682, 1940.

TABLE I. - SUMMARY OF DESIGN PARAMETERS

| | Solid blade | Tandem blades |
|---|---|---|
| Total camber, $\varphi_T$, deg | 58.8 | 58.8 |
| Total chord, $C_T$, m | .102 | .102 |
| Maximum thickness-chord ratio, $T_{max}/C_T$: | .08 | ------- |
| Front segment, $T_{max,F}/C_F$ | ------- | .08 |
| Rear segment, $T_{max,R}/C_R$ | ------- | .08 |
| Leading-edge radius-chord ratio, $R_i/C_T$: | .01 | ------- |
| Front segment, $R_{i,F}/C_F$ | ------- | .01 |
| Rear segment, $R_{i,R}/C_R$ | ------- | .01 |
| Trailing-edge radius-chord ratio, $R_o/C_T$: | 0.0075 | ------- |
| Front segment, $R_{o,F}/C_F$ | ------- | 0.0075 |
| Rear segment, $R_{o,R}/C_R$ | ------- | 0.0075 |
| Inlet fluid angle, $\beta_1$, deg (design point) | 43.25 | 43.25 |
| Incidence angle, i, deg (design point) | -3.0 | -3.0 |
| Overall blade solidity, $\sigma$ | 1.5 | 1.5 |
| Diffusion factor, D | .5 | ------- |

TABLE II. - GEOMETRIC CONFIGURATION OF TANDEM BLADES

| Chord ratio, $C_R/C_F$ | Camber ratio, $\varphi_R/\varphi_F$ | Gap, $G/C_T$ | Overlap, $L/C_T$ | Convergence, F | Rear-segment setting angle, $\kappa_{b\text{-}b}$, deg | Front camber, $\varphi_F$, deg | Rear camber, $\varphi_R$, deg | Front-segment chord length, $C_F/C_T$ | Rear-segment chord length, $C_R/C_T$ |
|---|---|---|---|---|---|---|---|---|---|
| Effect of chord ratio | | | | | | | | | |
| 1 | 3 | 0.04 | 0.11 | 1.1 | -5.7 | 17.0 | 50.9 | 0.56 | 0.56 |
| 1.5 | ↓ | ↓ | ↓ | ↓ | -3.9 | 16.7 | 50.1 | .45 | .67 |
| 2 | | | | | -2.6 | 16.6 | 49.8 | .37 | .75 |
| 3 | | | | | -.55 | 16.5 | 49.5 | .29 | .83 |
| Effect of camber ratio | | | | | | | | | |
| 2 | 2 | 0.04 | 0.11 | 1.2 | -3.4 | 23.1 | 46.1 | 0.37 | 0.74 |
| 2 | 3 | .04 | .11 | 1.2 | -4.8 | 17.2 | 51.6 | .37 | .74 |
| 2 | 4 | .04 | .11 | 1.2 | -5.5 | 13.7 | 54.8 | .37 | .75 |

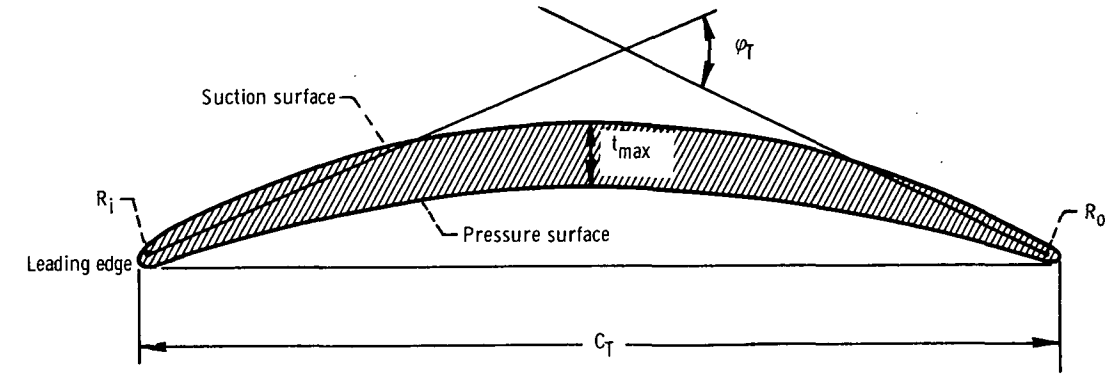


(a) Solid blade.

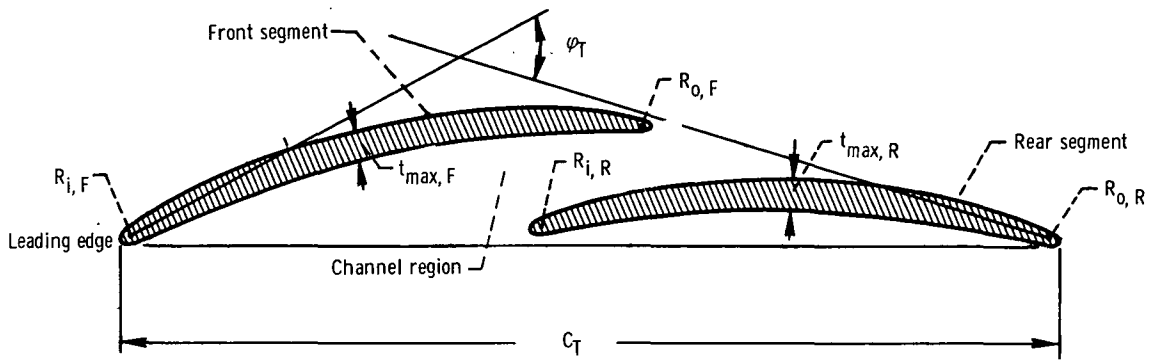


(b) Tandem blade.

Figure 1. - Nomenclature for solid and tandem blades.

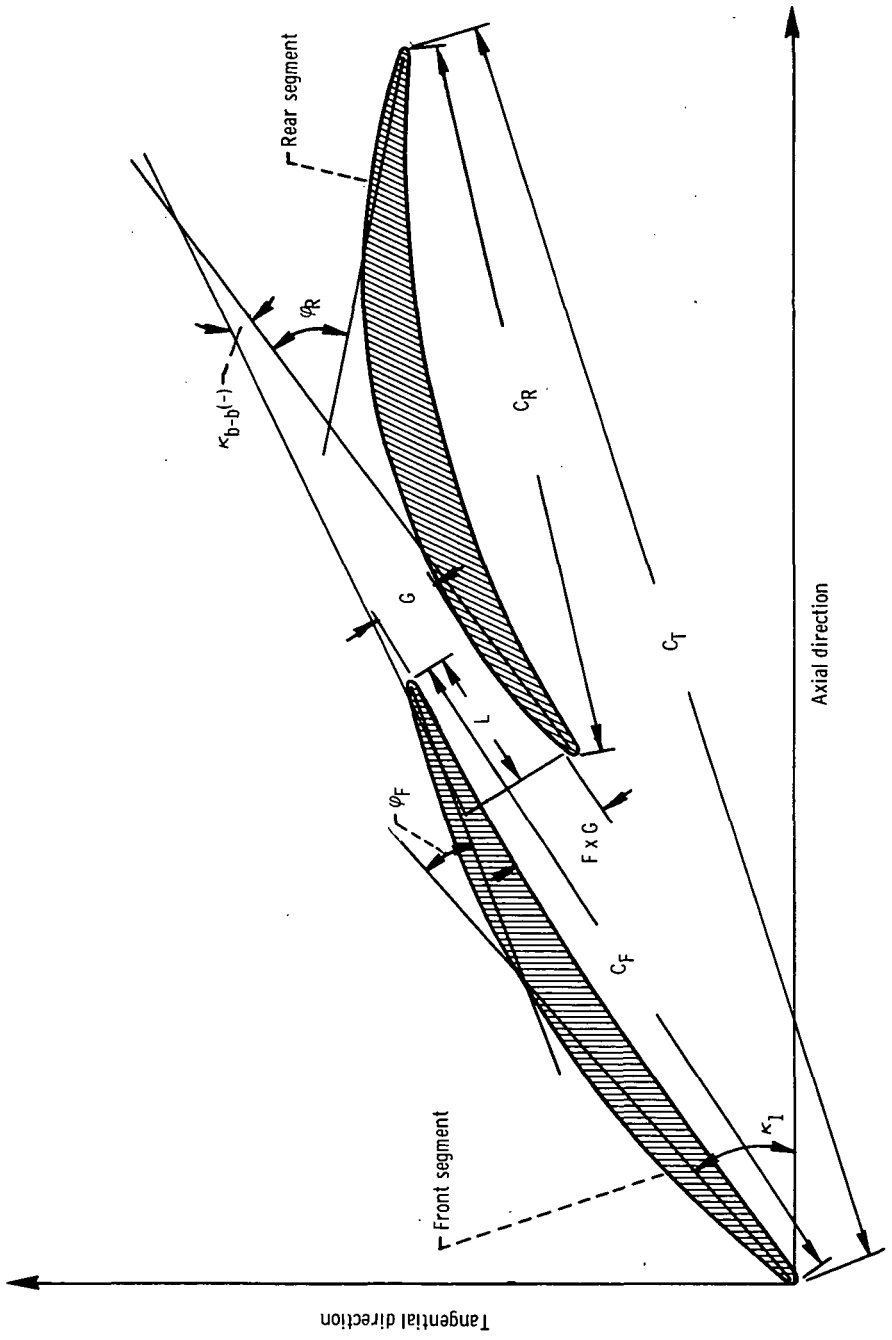


Figure 2. - Geometric variables for tandem blades.

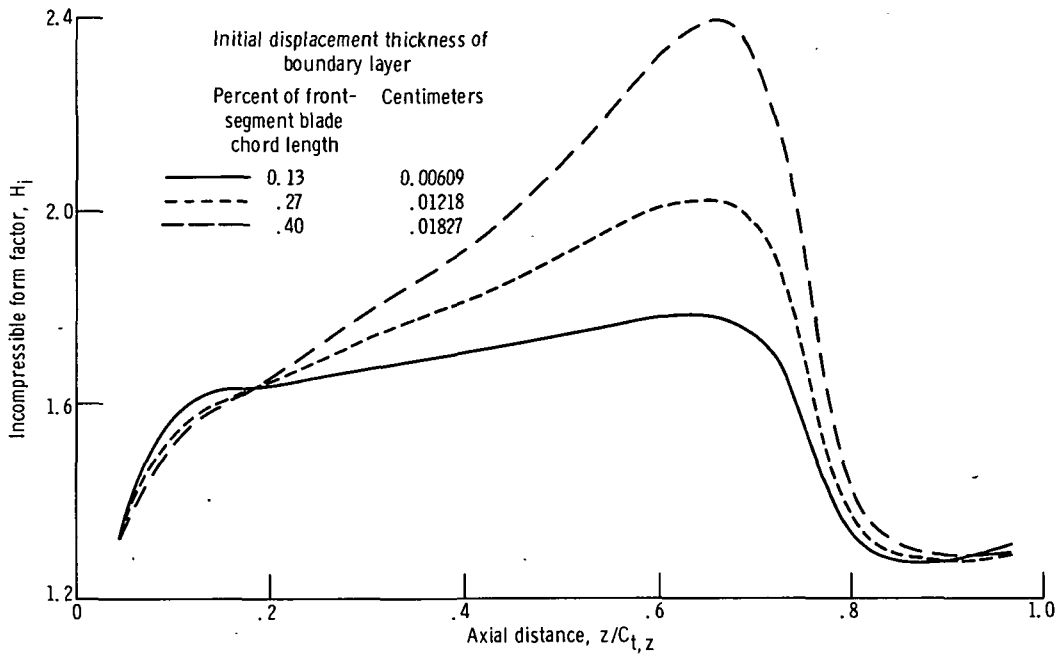


Figure 3. - Effect of initial displacement thickness on form factor - front-segment pressure surface of tandem blade.

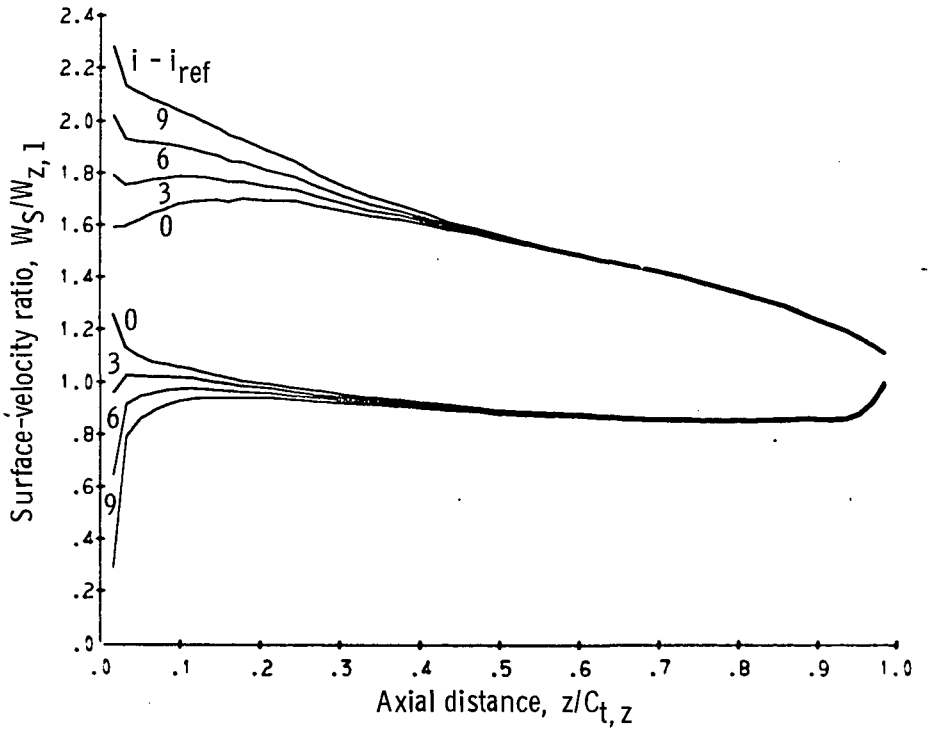


Figure 4. - Surface-velocity profile - solid blade.

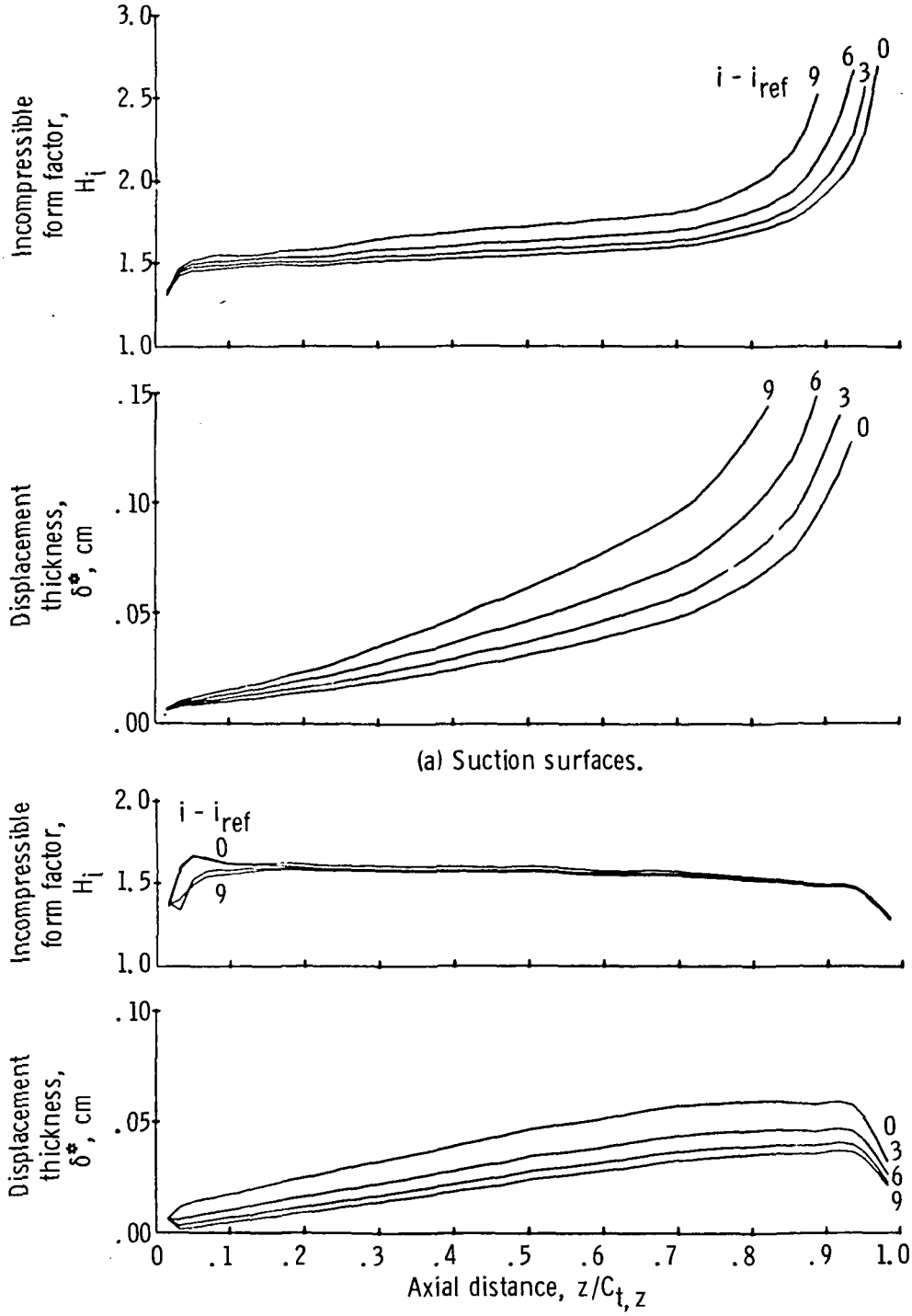


Figure 5. - Boundary-layer development - solid blade.

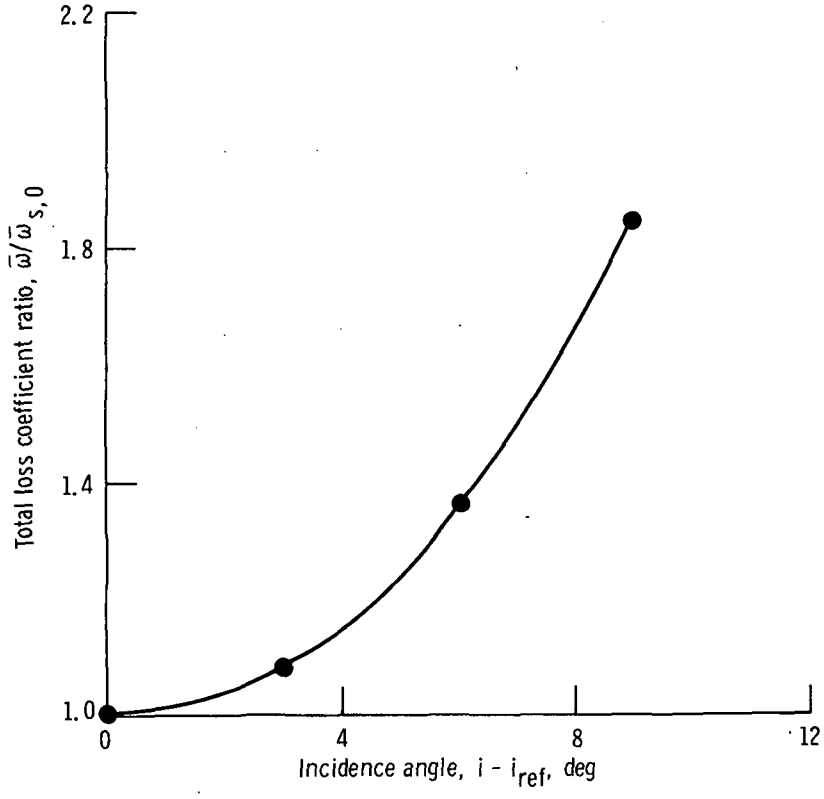


Figure 6. - Effect of incidence angle on solid blade section loss.

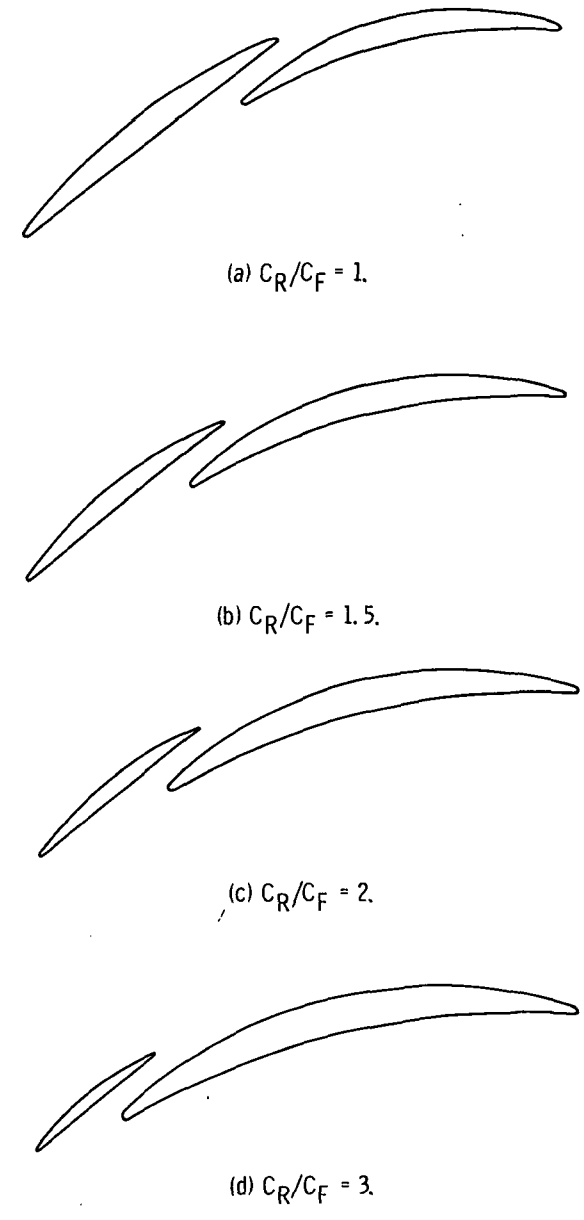

(a) $C_R/C_F = 1.$

(b) $C_R/C_F = 1.5.$

(c) $C_R/C_F = 2.$

(d) $C_R/C_F = 3.$

Figure 7. - Geometry of tandem blade section - chord ratio variation for constant camber ratio of 3.

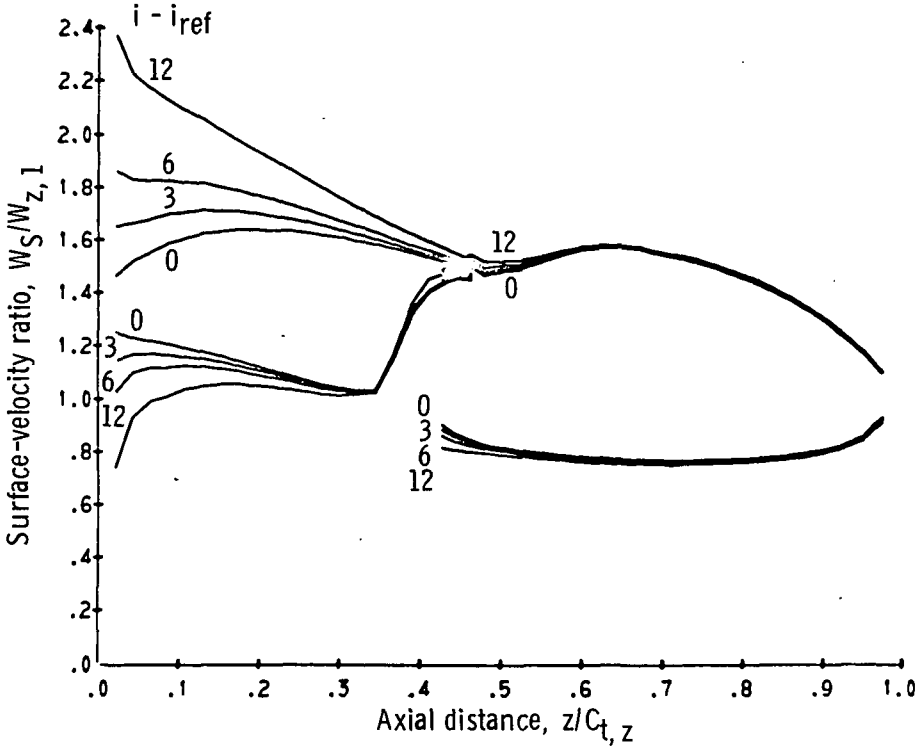


Figure 8. - Surface-velocity profile - chord ratio, 1.

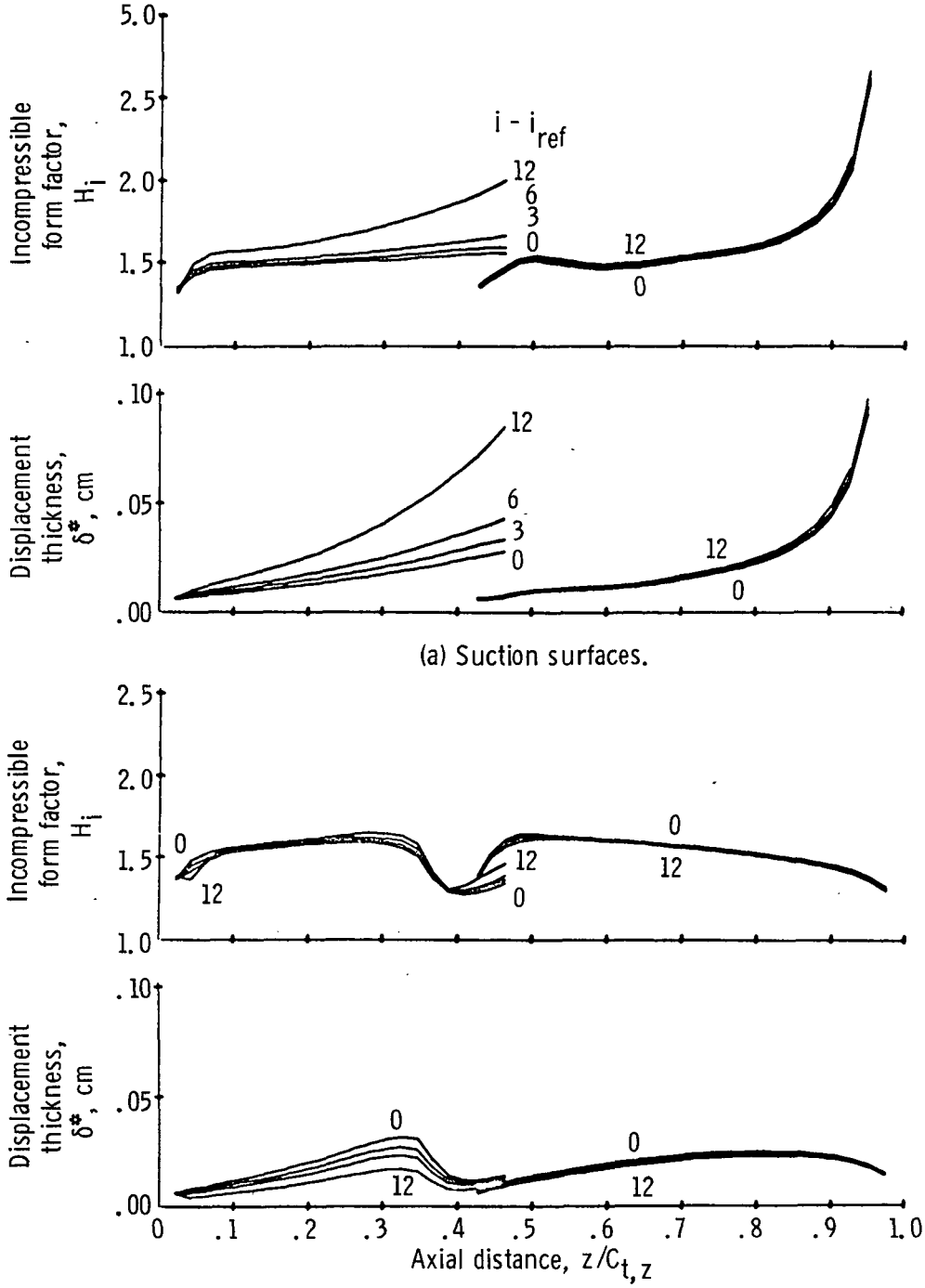


(a) Suction surfaces.

(b) Pressure surfaces.

Figure 9. - Boundary-layer development - chord ratio, 1.

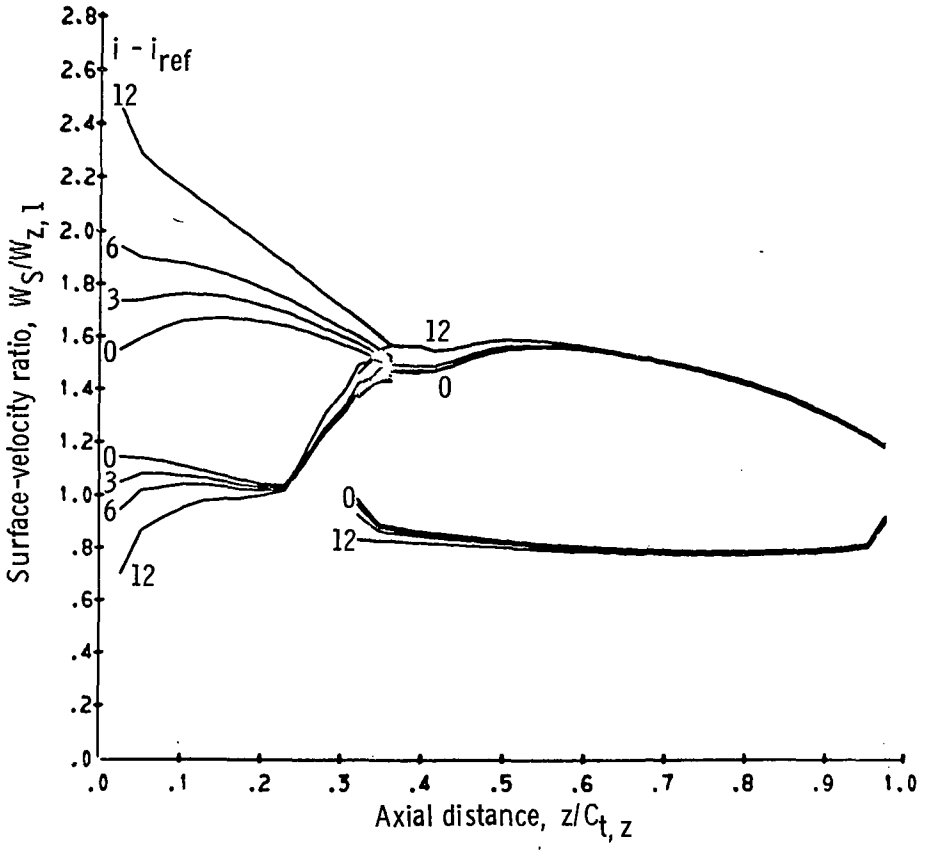


Figure 10. - Surface-velocity profile - chord ratio, 1.5.

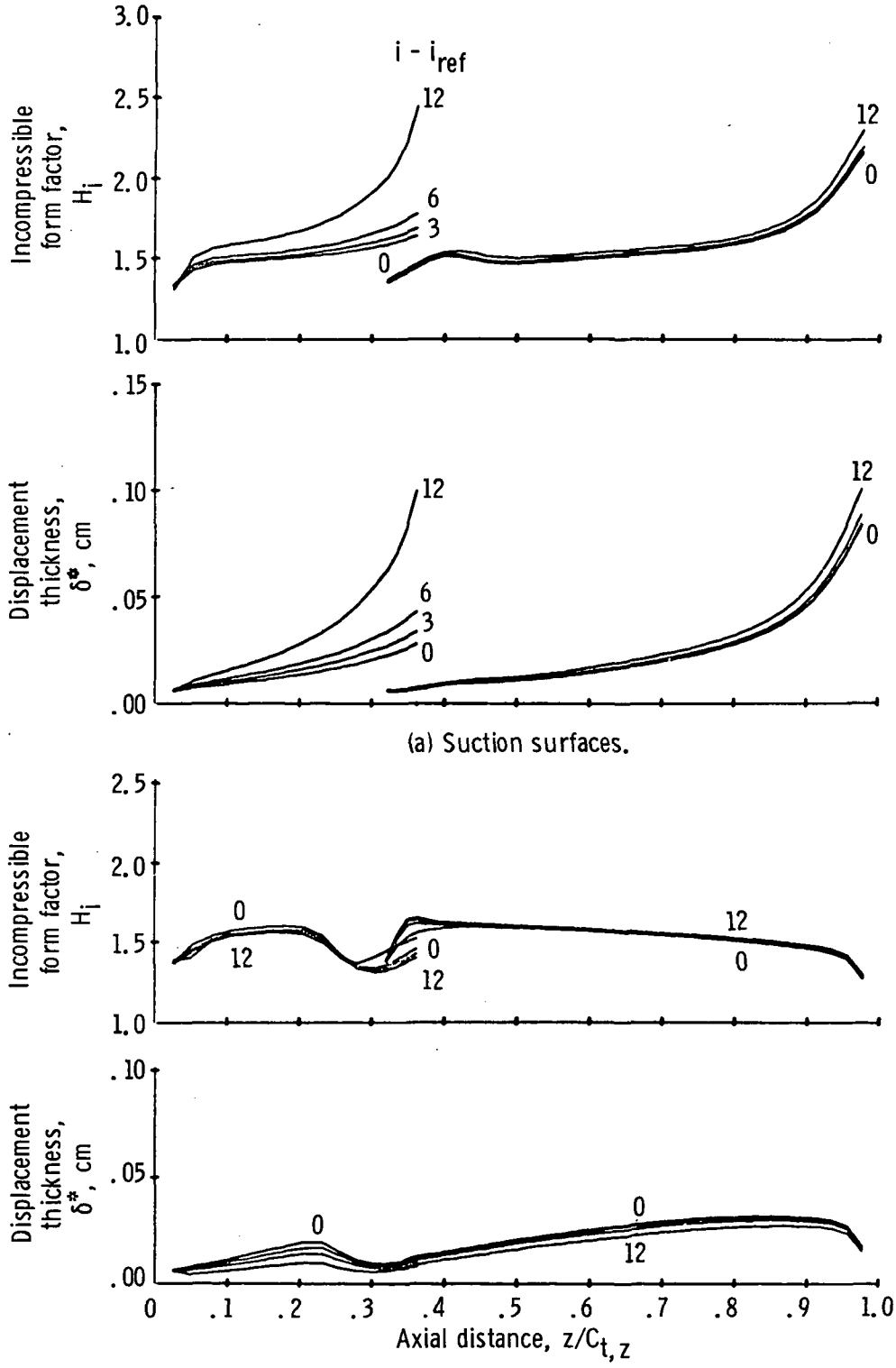


Figure 11. - Boundary-layer development - chord ratio, 1.5.

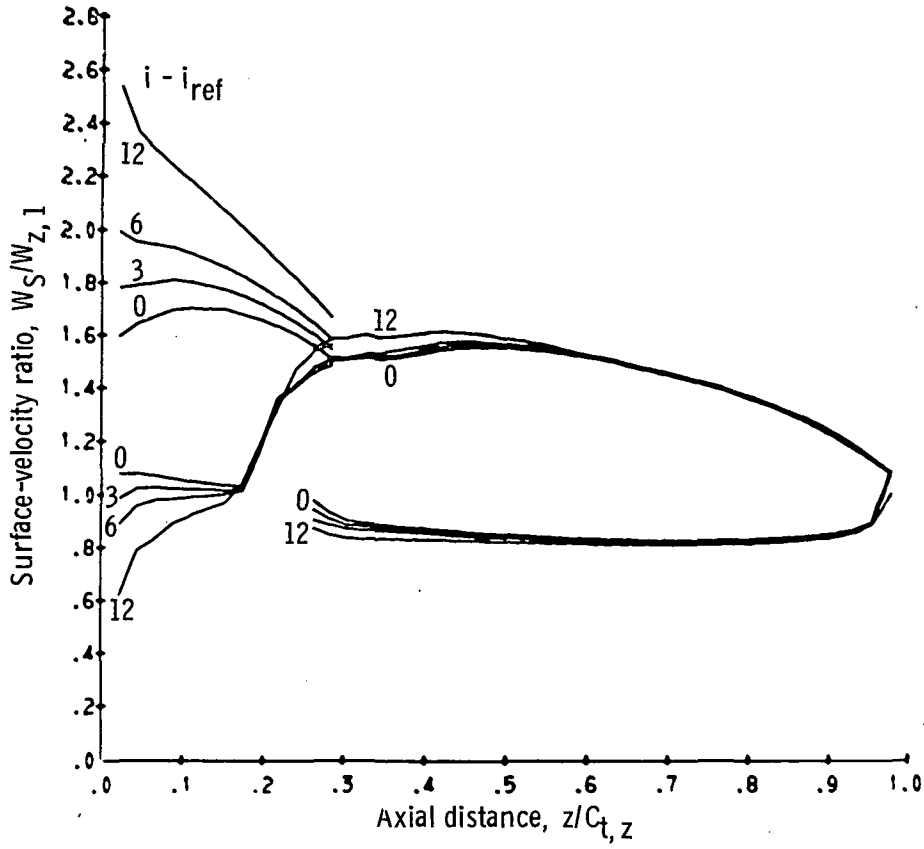


Figure 12. - Surface-velocity profile - chord ratio, 2.

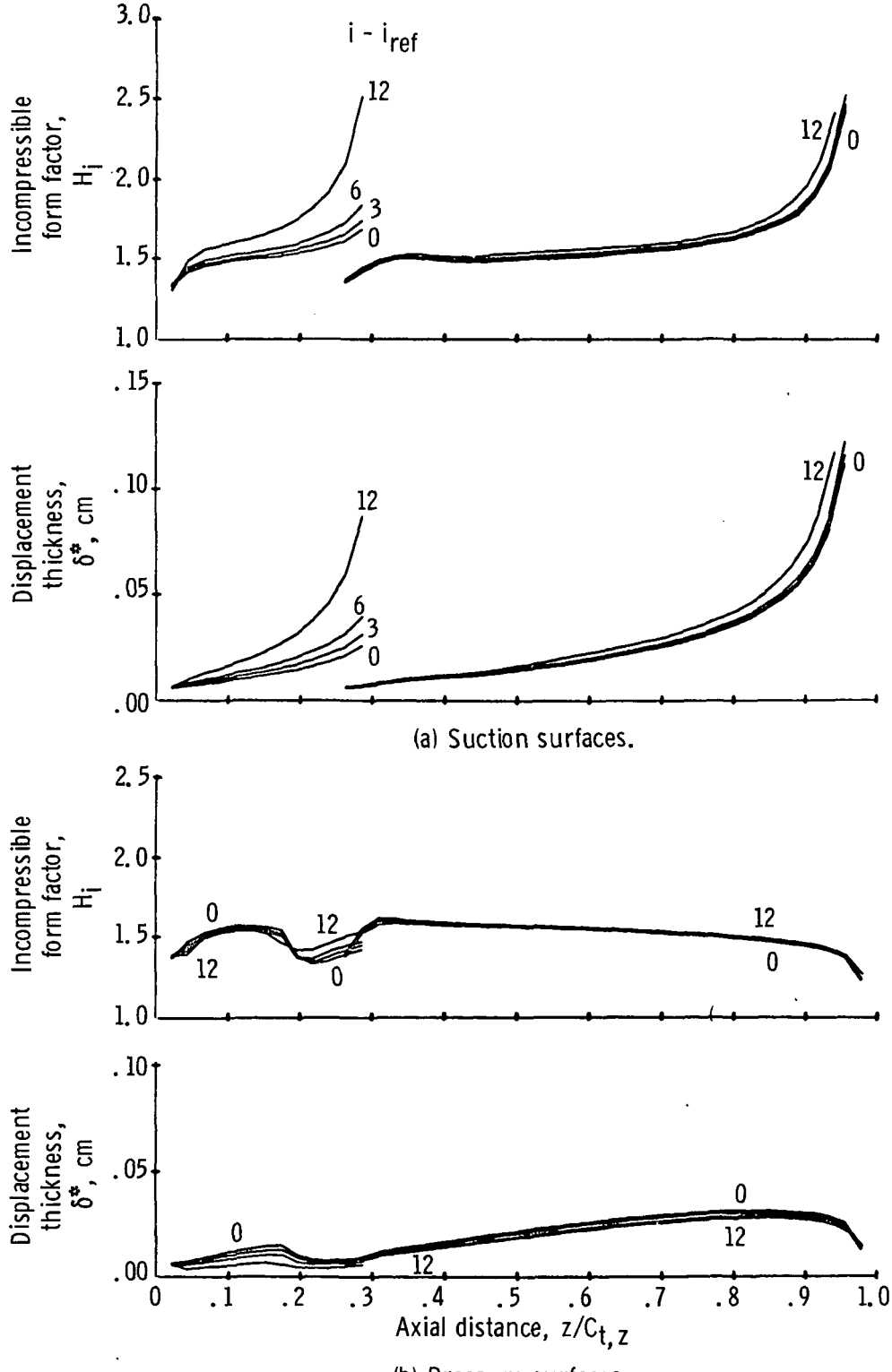


Figure 13. - Boundary-layer development - chord ratio, 2.

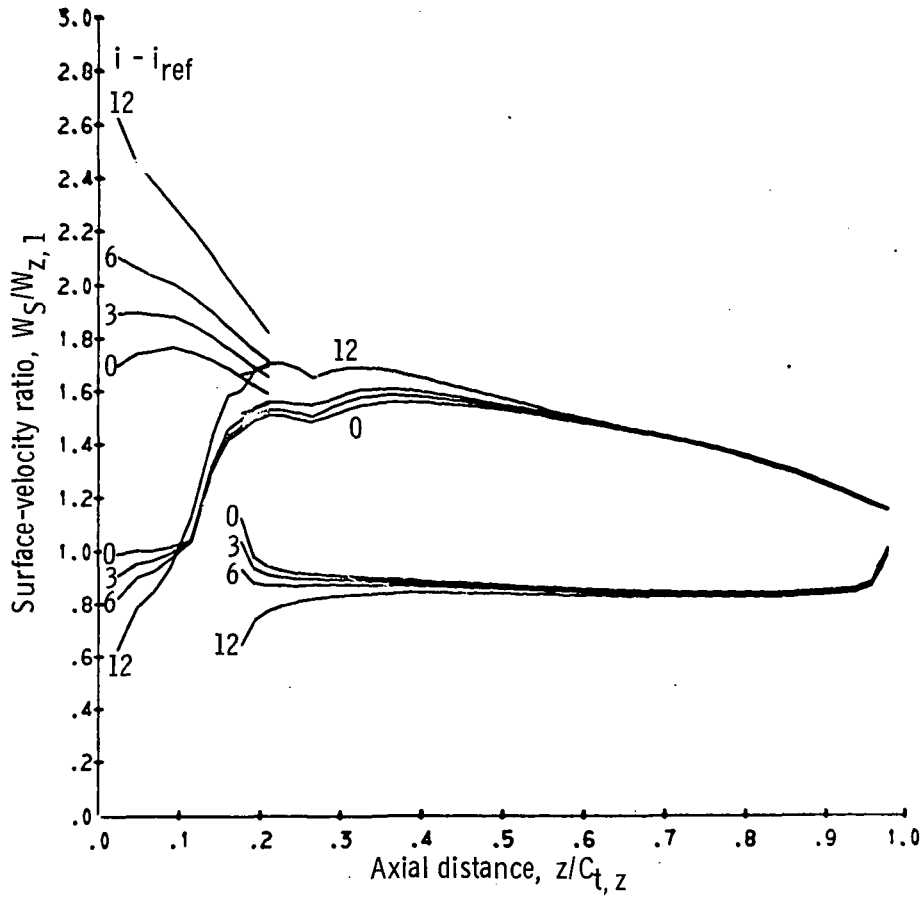


Figure 14. - Surface-velocity profile - chord ratio, 3.

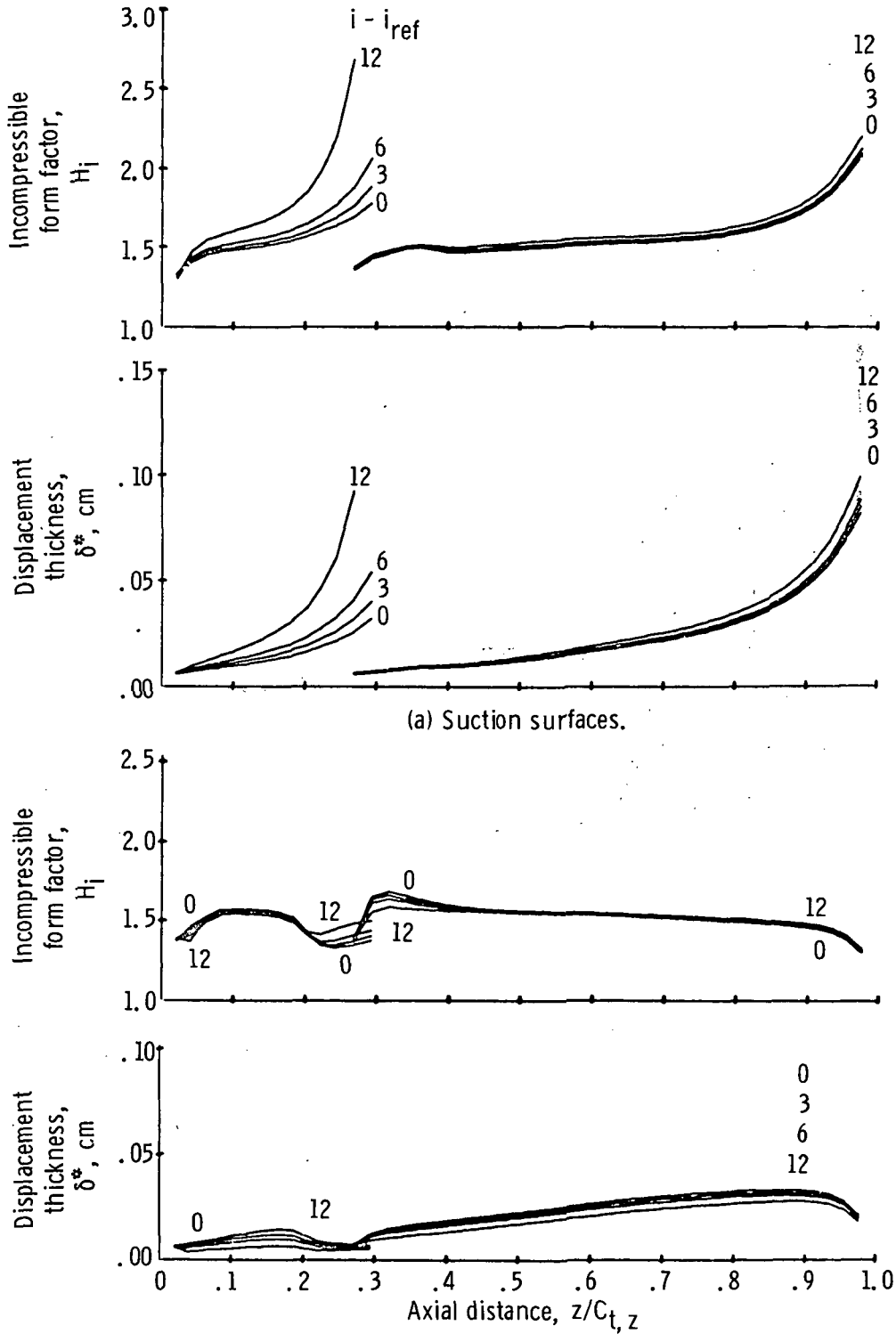


Figure 15. - Boundary-layer development - chord ratio, 3.

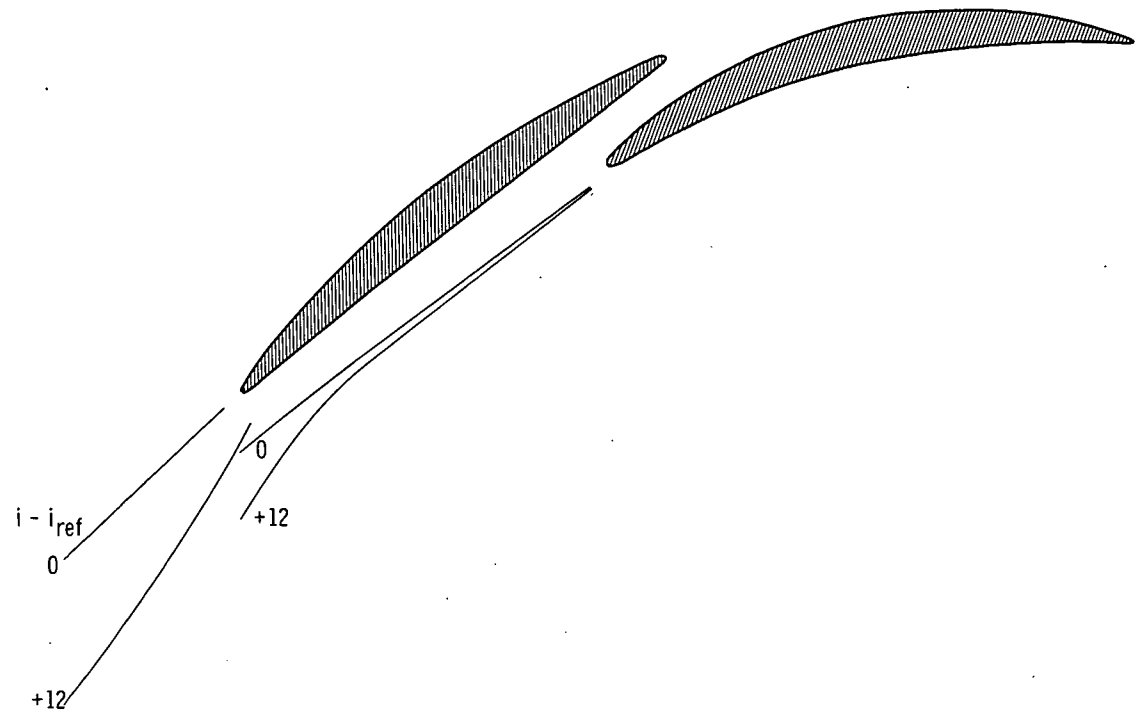


(a) Chord ratio, 1.

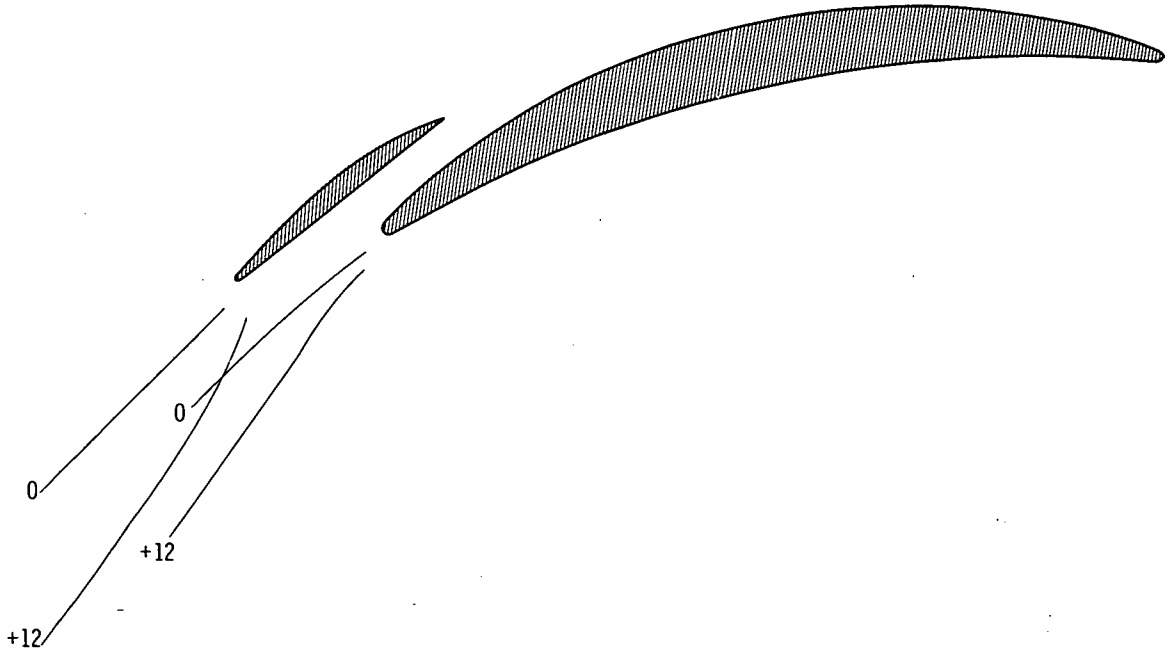


(b) Chord ratio, 3.

Figure 16. - Guidance effect of front segment on stagnation streamlines.

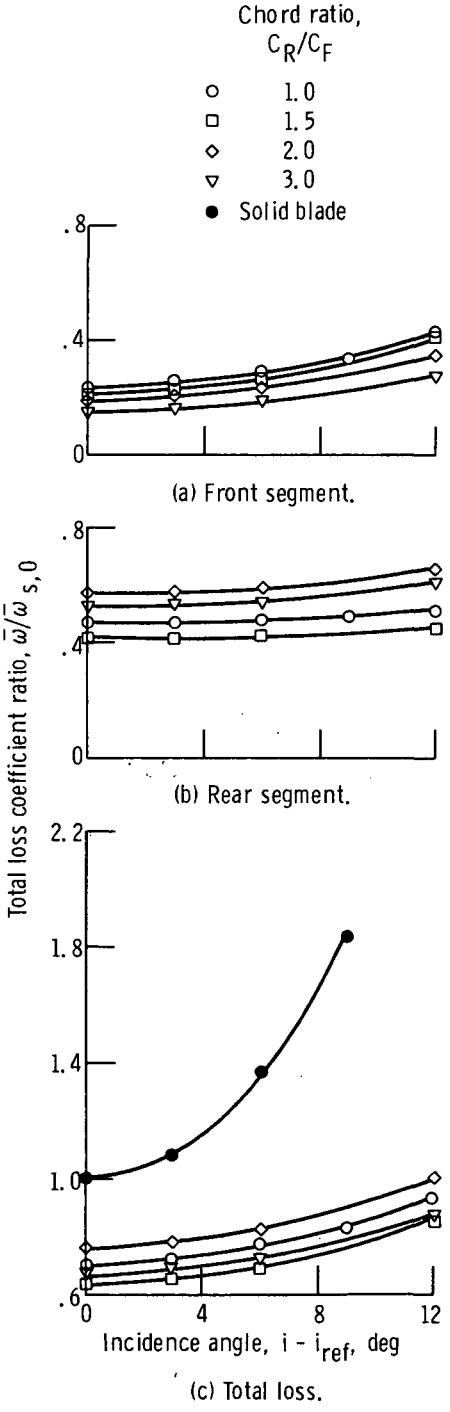


Figure 17. - Effect of incidence angle on loss coefficient for different chord ratio configurations.

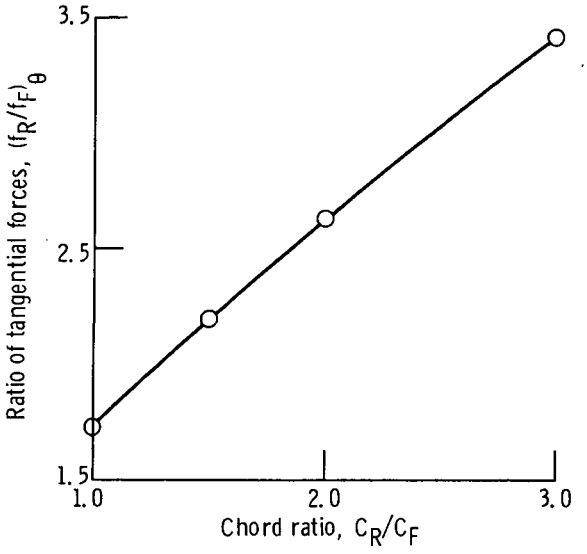


Figure 18. - Effect of chord ratio on loading split.

(a) $\varphi_R/\varphi_F = 2$.

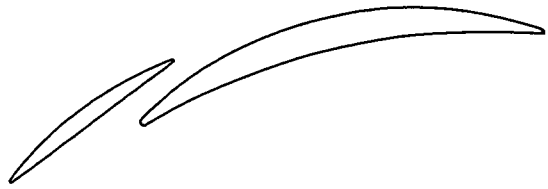

(b) $\varphi_R/\varphi_F = 3$.

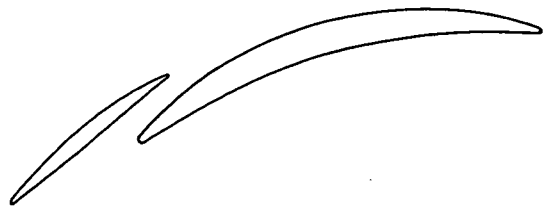

(c) $\varphi_R/\varphi_F = 4$.

Figure 19. - Geometry of tandem blade section - camber ratio variation for constant chord ratio of 2.

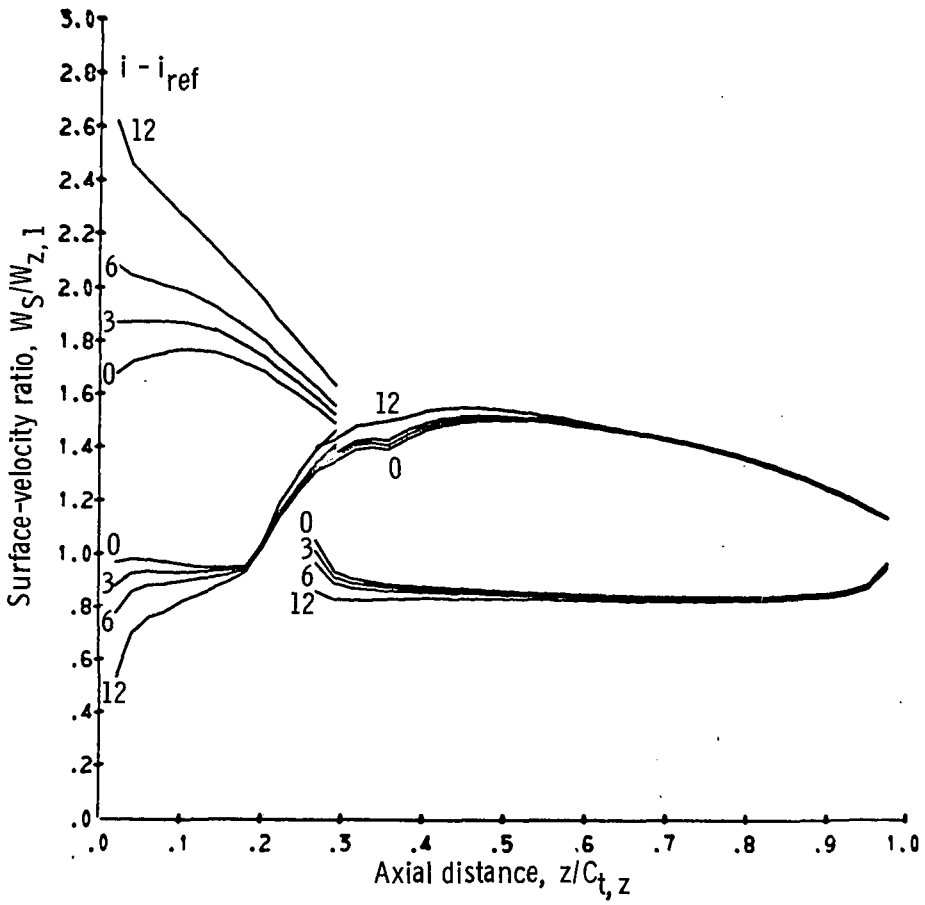


Figure 20. - Surface-velocity profile - camber ratio, 2.

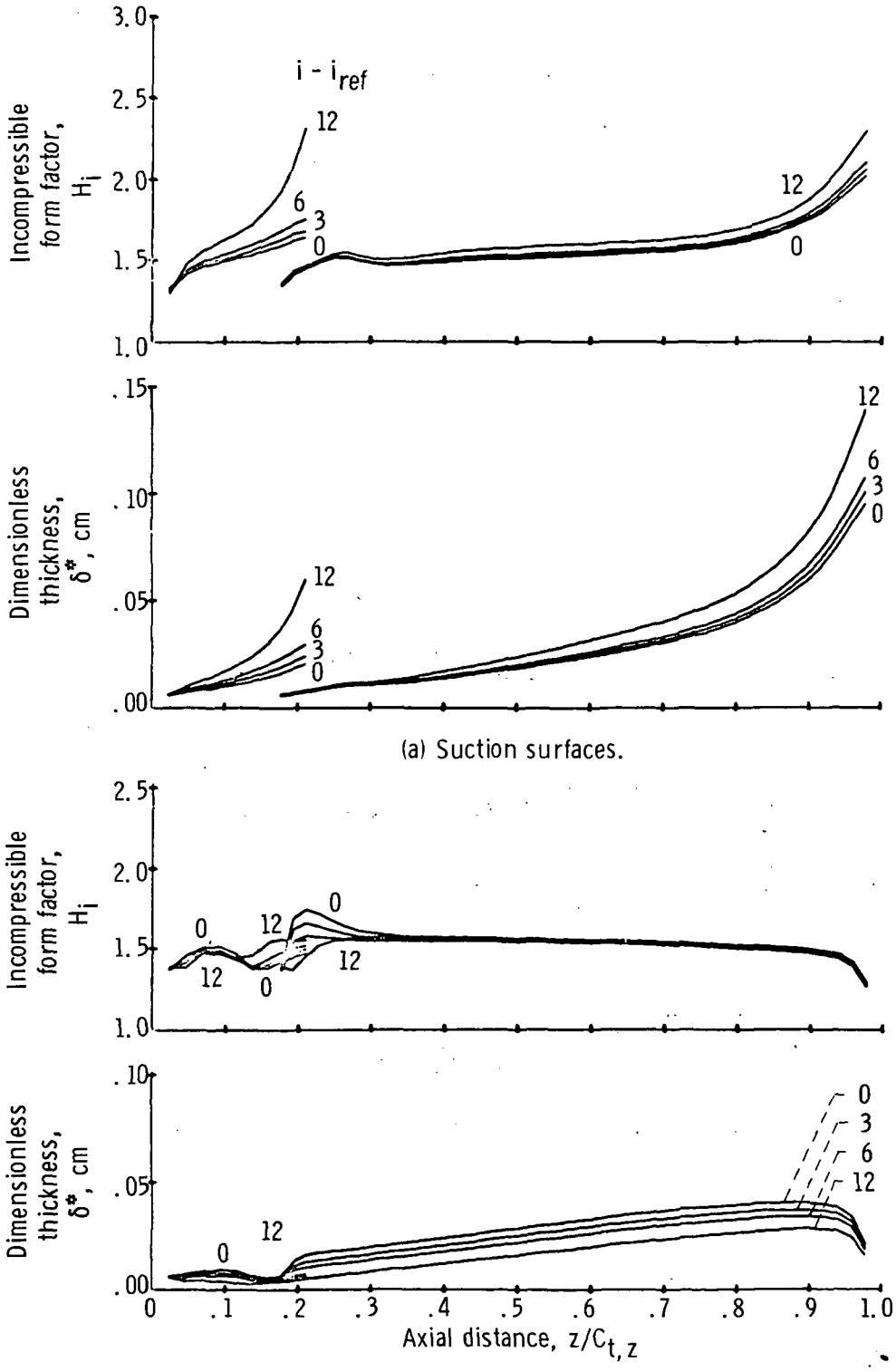


Figure 21. - Boundary-layer development - camber ratio, 2.

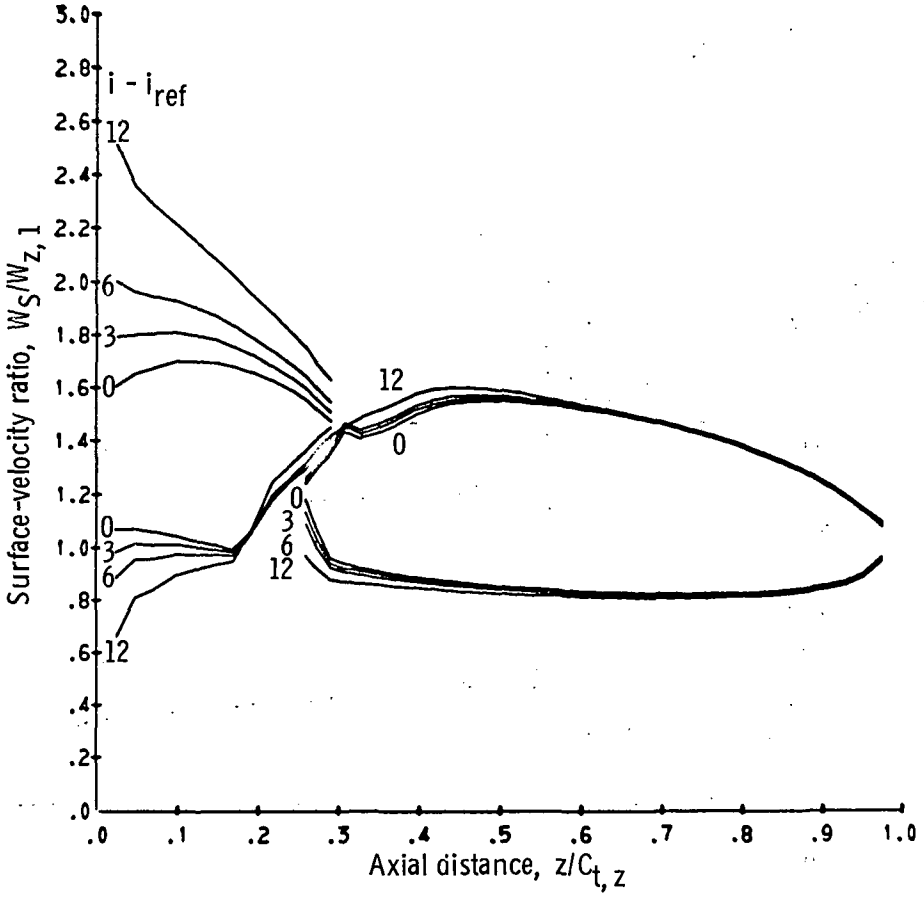


Figure 22. - Surface-velocity profile - camber ratio, 3.

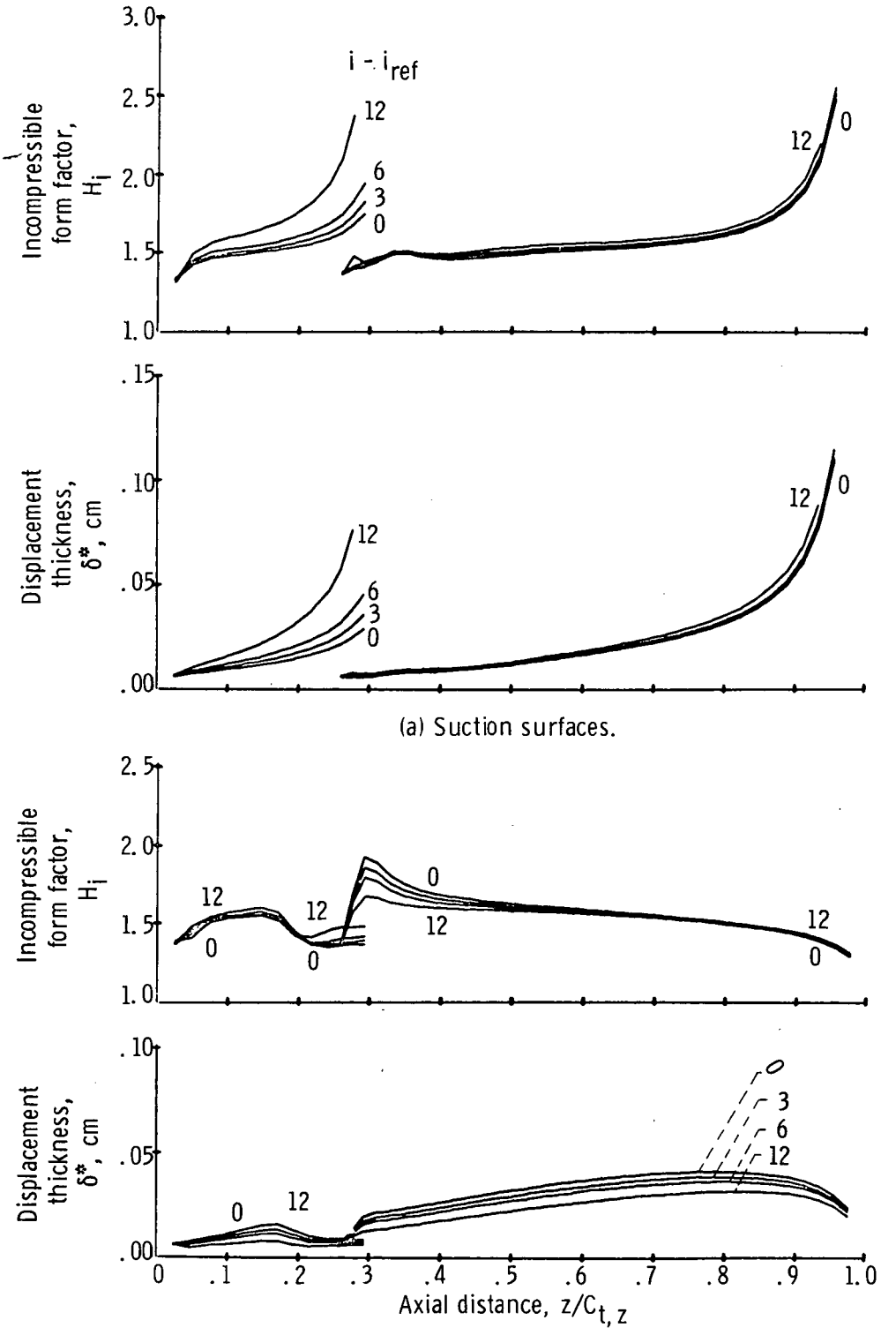


Figure 23. - Boundary-layer development - camber ratio, 3.

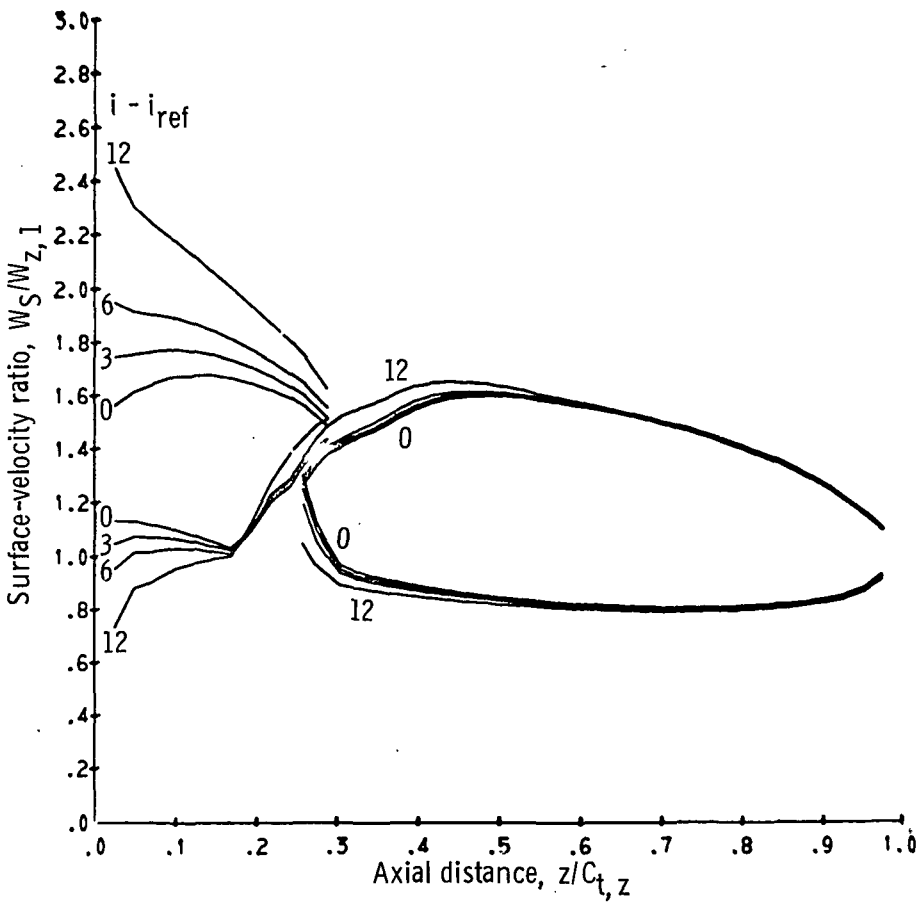


Figure 24. - Surface-velocity profile - camber ratio, 4.

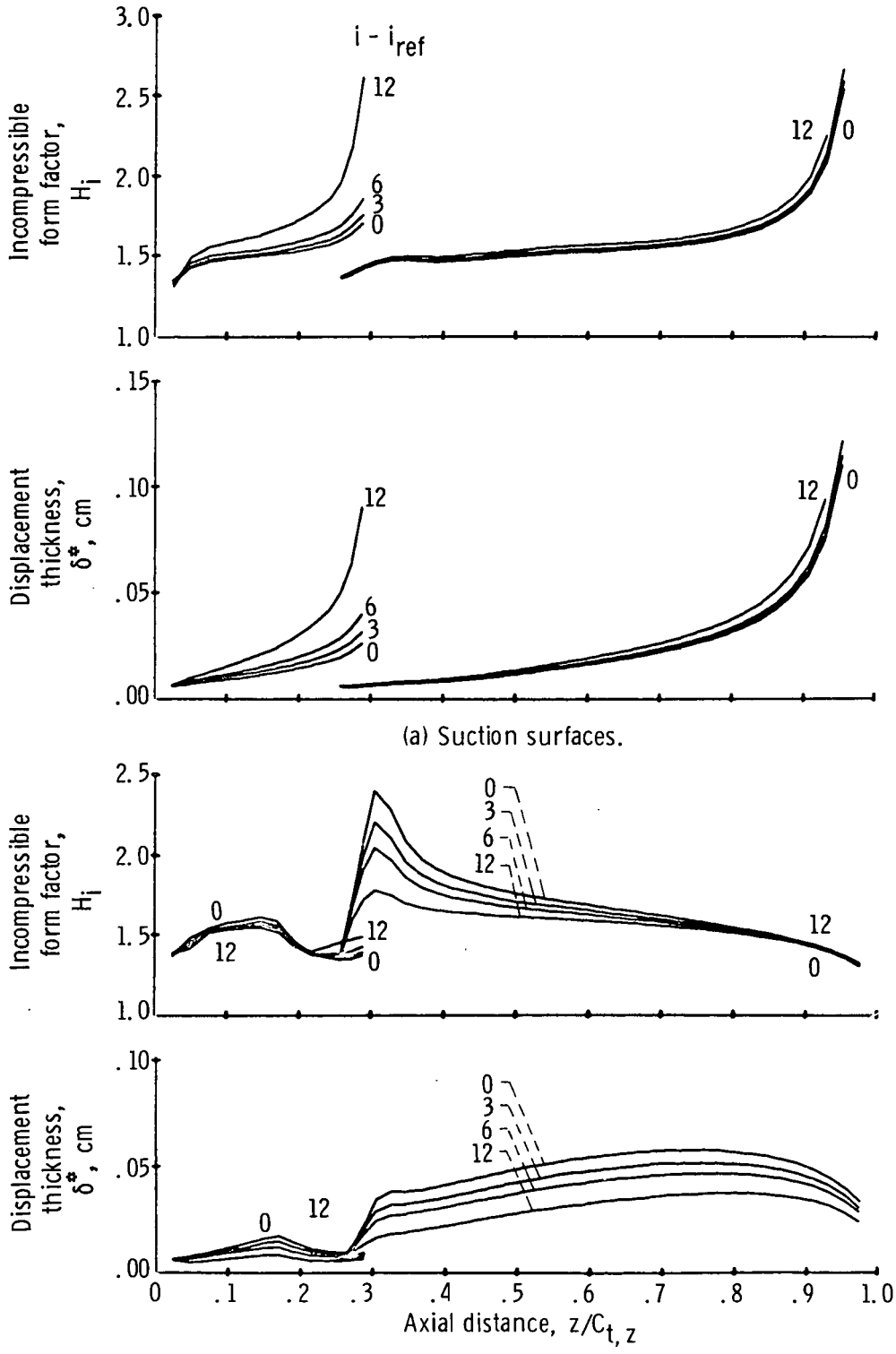


(a) Suction surfaces.

(b) Pressure surfaces.

Figure 25. - Boundary-layer development - camber ratio, 4.

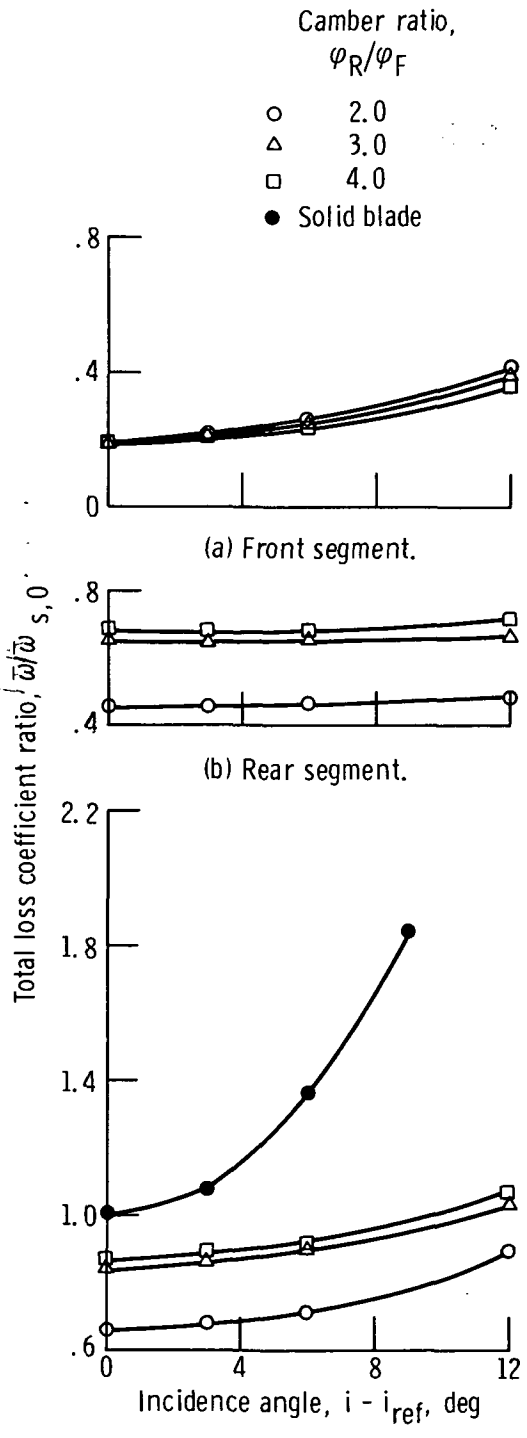


Figure 26. - Effect of incidence angle on loss coefficient for different camber ratio configurations.

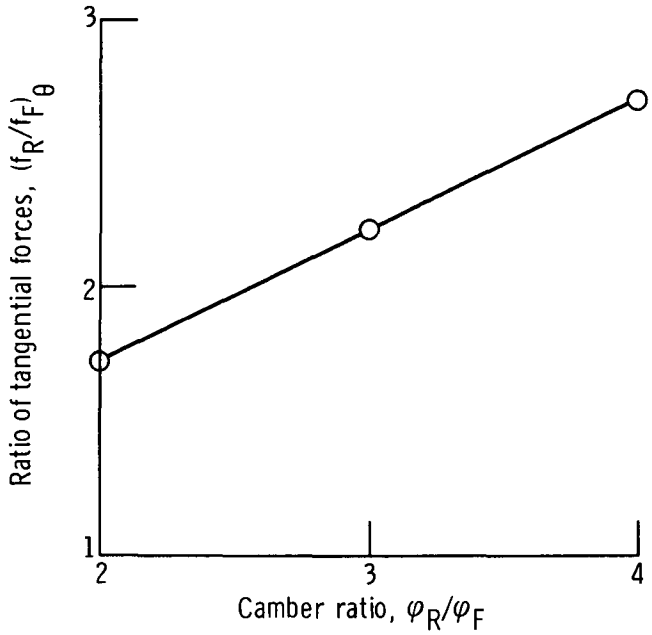


Figure 27. - Effect of camber ratio on loading split.

NATIONAL AERONAUTICS AND SPACE ADMINISTRATION
WASHINGTON, D.C. 20546

OFFICIAL BUSINESS
PENALTY FOR PRIVATE USE $300

SPECIAL FOURTH-CLASS RATE BOOK

POSTAGE AND FEES PAID
NATIONAL AERONAUTICS AND SPACE ADMINISTRATION
451

U.S.MAIL

POSTMASTER: If Undeliverable (Section 158 Postal Manual) Do Not Return

*"The aeronautical and space activities of the United States shall be conducted so as to contribute . . . to the expansion of human knowledge of phenomena in the atmosphere and space. The Administration shall provide for the widest practicable and appropriate dissemination of information concerning its activities and the results thereof."*

—NATIONAL AERONAUTICS AND SPACE ACT OF 1958

# NASA SCIENTIFIC AND TECHNICAL PUBLICATIONS

TECHNICAL REPORTS: Scientific and technical information considered important, complete, and a lasting contribution to existing knowledge.

TECHNICAL NOTES: Information less broad in scope but nevertheless of importance as a contribution to existing knowledge.

TECHNICAL MEMORANDUMS: Information receiving limited distribution because of preliminary data, security classification, or other reasons. Also includes conference proceedings with either limited or unlimited distribution.

CONTRACTOR REPORTS: Scientific and technical information generated under a NASA contract or grant and considered an important contribution to existing knowledge.

TECHNICAL TRANSLATIONS: Information published in a foreign language considered to merit NASA distribution in English.

SPECIAL PUBLICATIONS: Information derived from or of value to NASA activities. Publications include final reports of major projects, monographs, data compilations, handbooks, sourcebooks, and special bibliographies.

TECHNOLOGY UTILIZATION PUBLICATIONS: Information on technology used by NASA that may be of particular interest in commercial and other non-aerospace applications. Publications include Tech Briefs, Technology Utilization Reports and Technology Surveys.

***Details on the availability of these publications may be obtained from:***

**SCIENTIFIC AND TECHNICAL INFORMATION OFFICE**

**NATIONAL AERONAUTICS AND SPACE ADMINISTRATION**

**Washington, D.C. 20546**